

The Bowen–Series coding and zeros of zeta functions

Mark Pollicott

Polina Vytnova*

Abstract

We give a discussion of the classical Bowen–Series coding and, in particular, its application to the study of zeta functions and their zeros. In the case of compact surfaces of constant negative curvature $\kappa = -1$ the analytic extension of the Selberg zeta function to the entire complex plane is classical, and can be achieved using the Selberg trace formula. However, an alternative dynamical approach is to use the Bowen–Series coding on the boundary at infinity to construct a piecewise analytic expanding map from which the extension of the zeta function can be obtained using properties of the associated transfer operator. This latter method has the advantage that it also applies in the case of infinite area surfaces provided they don’t have cusps. For such examples the location of the zeros is somewhat more mysterious. However, in particularly simple cases there is a striking structure to the zeros when we take appropriate rescaling. We will try to give some insight into this phenomenon.

Contents

1	Introduction	3
2	Two types of dynamical system	4
3	Hyperbolic Geometry	8
4	Fuchsian groups and the Bowen–Series map	9
4.1	Fuchsian groups	9
4.2	Bowen–Series map	10

*The first author was partly supported by ERC-Advanced Grant 833802-Resonances and EPSRC grants EP/W033917/1 and EP/V053663/1. The authors would like to thank the organizers of the Simons Semester program “Topological, smooth and holomorphic dynamics, ergodic theory, fractals” for the financial support and hospitality. The authors are also grateful to the organizers of the program at SUSTech in Shenszen (China) and to the head of the mathematics department Jeff Xia for their help and hospitality.

5	Dynamical Applications: Compact surfaces	13
5.1	Counting closed geodesics	13
5.2	Taking a leaf out of the number theory book	14
5.3	Error terms in counting closed geodesics	15
5.4	The Banach spaces	17
5.5	Mixing of geodesic flow	18
6	The Bowen–Series map for infinite area surfaces	20
7	Dynamical applications: non-compact surfaces	22
7.1	Counting closed geodesics	22
7.2	The Banach spaces	23
7.3	Measures and mixing	25
8	Location of resonances for infinite area surfaces	26
8.1	Rigorous results: the case of pair of pants	26
8.1.1	Distribution of zeros	26
8.1.2	Patterns of zeros	26
8.1.3	Approximating Selberg zeta function	29
8.2	The case of one-holed torus	31
8.2.1	Plots of zeros and conjectures	31
8.2.2	Geometry of a one-holed torus	36
8.2.3	Approximating determinant	38
8.2.4	Zeros of the determinant	44

Background. Some useful references for the basic material in these lectures are contained in the following books and articles. We will not cover even a fraction of all of the material in these sources, but that does not detract from their interest. The selection reflects the theme we are trying to give to the story we are telling.

1. Introductory reading: A lot of the foundational material can be found in a very accessible form in the Proceedings of the Trieste Conference on *Ergodic Theory, symbolic dynamics and hyperbolic dynamics* from 1989 [4].
2. Ergodic theory: The LMS lecture notes series volume by Nicholls [29].
3. Trace formulae: The very readable article of McKean on the use of heat kernels [24] and a monograph by Buser [9].
4. Resonance-free regions and density of resonances: two articles of Naud [27] and [28].
5. Since the notes were originally written, a book by Borthwick [6] and a book by Dyatlov and Zworski [14] appeared.

1 Introduction

Dynamical systems and ergodic theory are both subjects rich in concrete examples. To set the scene for these notes we will consider two basic examples of two somewhat different types of dynamical systems. The first is an example of a discrete dynamical system (or map) associated to an \mathbb{Z}_+ -action and corresponds to an expanding map on a disjoint union of intervals. This example has the virtue of being both simple and accessible. The second will be an example of a continuous dynamical system (or flow) associated to an \mathbb{R} -action and corresponds to the classical example of the geodesic flow for a surface of constant negative curvature. This example has been of paramount importance in the original development of ideas in ergodic theory, particularly in the 1930s.

Both of these examples, the map and the flow, have been the subject of extensive research. However, as we will see later, these two systems are not as unrelated as they might at first appear. The basis for this connection is some elegant ideas in the work of Bowen and Series [7] (and a closely related approach appears in the work of Adler and Flatto [2]). Unfortunately, the history of the theory is tinged with sadness. Robert (Rufus) Bowen was a professor at the University of California at Berkeley. During the collaboration with Caroline Series he died suddenly, at the age of 31. Their joint work was completed by his co-author and published posthumously in a memorial volume of *Publications Mathématiques (IHES)* dedicated to Bowen. Caroline served as the President of the London Mathematical Society in 2018–2022.

There have been other ways to associate to a geodesic flow an expanding map. Perhaps the best known is that of Ratner, which she subsequently generalised to Anosov flows. Later the construction was further generalised by Bowen to Axiom A flows (which were introduced by Smale, his supervisor in Berkeley). This method used two-dimensional Markov sections transferred along the flow direction, with obtained “parallelepipeds” playing the role of flow boxes. The associated Markov map corresponds to the interval map induced from the Poincaré map between sections by collapsing them along the stable direction (an observation which, at least, is made explicit in a paper of Ruelle [35]). However, the resulting interval map is not canonical, as one would anticipate from its potentially greater generality.

On the other hand, the Bowen–Series coding is very closely related to the generators of the fundamental group of the surface. Although the choice of generators is not unique, this leads to a very natural approach to understanding orbits. Indeed, a part of the appeal of the Bowen–Series coding is its transparency. The work of Bowen and Series pre-dated later work of Cannon and others on the automatic structure of more general Gromov hyperbolic groups, which is in a similar spirit.

The Bowen–Series coding has proved to be very useful in a number of different applications. This is particularly true when an explicit understanding of the fundamental group plays a role. The Selberg zeta function takes into account precisely one closed geodesic in each conjugacy class of the fundamental group.

In Section 8 we shall consider an application of one of the simplest cases of such coding,

for a three funnelled surface or a “pair of pants” and for a one-holed torus, to the study of resonances of the associated Selberg zeta function. To complete the introduction we summarize what we want to do, in a nutshell.

Aim of the note: To explore which results/methods (particularly in the context of zeta functions) carry over from the case of compact surface V to a surface V having infinite area using the Bowen–Series coding.

2 Two types of dynamical system

We now compare these two types of dynamics.

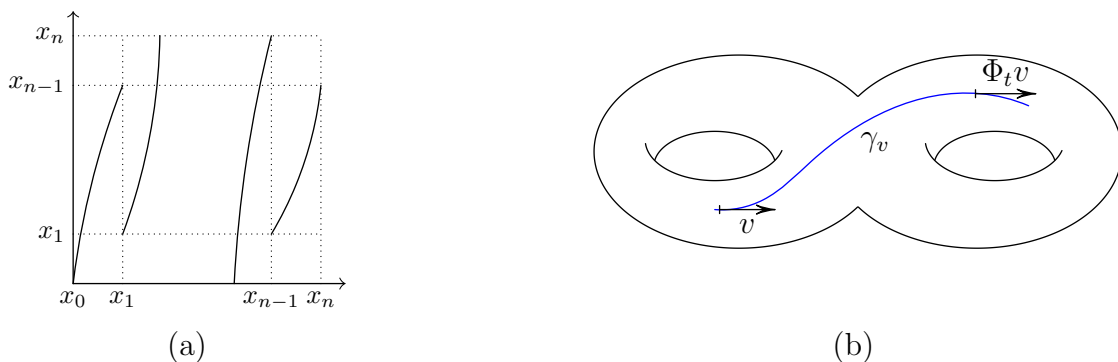


Figure 1: (a) A Markov expanding map of the interval. (b) The geodesic flow on the unit tangent bundle of a compact surface of constant negative curvature.

We list corresponding properties of the 1d map and the flow in Table 1. The folklore Lemma 1 on existence and uniqueness of the invariant measure has been variously attributed to: Bowen (1979), Adler (1972), Flatto (1969), Weiss (1968), Sinai (1968) and Renyi (1960). For an interesting historical perspective we refer the reader to [1].

Of course there are various classical results we are implicitly using. For example, we will assume that the surface V is orientable and has genus at least 2 (or, equivalently, negative Euler characteristic). This ensures that V can carry a metric of negative curvature. Moreover, there is a number of obvious generalisations that we will not consider. For example, the analogous results in the case of surfaces of variable negative curvature.

Having emphasized the parallels between these two systems, we can look for a more tangible connection. More precisely, we can pose the following question.

Question 1. How can we relate the Markov map and the geodesic flow?

One elegant solution to this problem appears in the work of Bowen and Series [7], as mentioned in the introduction, where an explicit construction is suggested. If we take a surface

Discrete (Interval maps)	Continuous (Geodesic flows)
Consider a partition of the unit interval $X = \bigcup_{j=0}^{n-1} I_j$, where $I_j = [x_j, x_{j+1}]$ and $0 = x_0 < x_1 < \dots < x_n = 1$	Consider a compact connected surface V with constant negative curvature $\kappa = -1$ such that the first homotopy group $\pi_1(V)$ is finitely generated. Let $Y = \{v \in TV : \ v\ = 1\}$ be the unit tangent bundle.
Let $T: X \rightarrow X$ be a piecewise smooth, uniformly expanding, Markov and transitive map, namely $T \in C^\infty(I_j)$; $\exists \beta > 1$ such that $\forall x \in X T'(x) \geq \beta$; $T(I_j)$ is a union of I_k ; $x \in X$ which orbit $\{T^n x\} \subseteq X$ is dense.	Let $\varphi_t: Y \rightarrow Y$ be the geodesic flow: $\forall v \in Y$ choose the unique geodesic $\gamma_v: \mathbb{R} \rightarrow V$ such that $\dot{\gamma}_v(0) = v$ and then define $\varphi_t v = \dot{\gamma}_v(t)$. This corresponds to parallel transport. The flow φ_t is transitive, i.e. $\exists v \in Y$ which orbit $\{\varphi_t v \in Y \mid t \in \mathbb{R}\}$ is dense.
Lemma 1 (Folklore). There exists a unique T -invariant probability measure, which is absolutely continuous with respect to the Lebesgue measure.	Lemma 2. Let $d\vartheta$ be the Lebesgue measure along the orbits of the flow. Then the Liouville measure $d\nu = d(\text{Vol})_V \times d\vartheta$ is invariant with respect to the geodesic flow φ_t .

Table 1: Correspondence between discrete and continuous dynamics.

of a fixed genus $g \geq 2$ then the associated expanding maps for the geodesic flow for different metrics on V will be topologically conjugate. However, the actual maps themselves will depend fundamentally on the choice of metric on the surface.

Recall that the universal cover of a compact connected surface V that carries a metric of constant negative curvature is the unit disk \mathbb{D} endowed with the hyperbolic metric; and the fundamental group $\pi_1(V)$ acts on the universal cover \mathbb{D} . The Bowen–Series construction rests on the idea of hyperfiniteness, i.e., the way the action

$$\pi_1(V) \times \partial\mathbb{D} \rightarrow \partial\mathbb{D}$$

of the fundamental group $\pi_1(V)$ on the boundary $\partial\mathbb{D}$ of the universal cover can be replaced by a single transformation. The Bowen–Series transformation is a specific realisation of such a phenomenon. It is defined as a map on the limit set, and more precisely is defined on a union of arcs which form a partition of the limit set. However, we can easily think of them as being maps of the interval, or maps on a Cantor set contained in an interval.

This approach has the advantage that complicated problems for the geodesic flow can often be reduced to simpler problems for the expanding map of the interval. We can summarise this method (elevated below to a “philosophy”) as follows.

Philosophy

1. Consider a problem for the geodesic flow $\varphi_t: Y \rightarrow Y$;
2. Reduce the problem to a problem for the associated expanding map $T: X \rightarrow X$;
3. Solve the problem for T (assuming one can!);
4. Relate it back to a solution for the original problem for $\varphi_t: Y \rightarrow Y$.

Of course, like all approaches its value probably ultimately depends on how useful it is. More precisely, we could ask:

Question 2. What sort of problems can one address?

One would naturally expect any useful technique to have many different applications, but for simplicity we could divide the types of problems we typically consider into two general classes:

Types of problems

- (a) *Topological*, such as properties of closed orbits). As a specific example we could consider results on the distribution of closed orbits which reflect information on their free homotopy classes (i.e., conjugacy classes in the fundamental group). The Bowen–Series coding makes it easy to relate the closed orbits for the flow to periodic orbits $\{x, Tx, \dots, T^{n-1}x\}$ (with $T^n x = x$) for the associated transformation. Furthermore, the usefulness of this particular coding is that the word length of the corresponding geodesic will be n , except in a finite number of exceptional cases.
- (b) *Measure theoretic*, such as properties of the invariant measures for the map and for the flow. The two measures are intimately related by the classical work of Bowen–Ruelle. For example, showing ergodicity for the flow automatically implies ergodicity for the discrete map. In the reverse direction, ergodicity for the discrete map, together with some modest hypothesis on the roof function, implies ergodicity for the flow. Stronger properties such as strong mixing, mixing rates, central limit theorems, etc. can be considered in each context, with varying degrees of complexity for the correspondence between them.

Since we are interested in ergodic theory and dynamical systems it is natural to use the model of the geodesic flow using expanding interval maps to try to understand its dynamics. However, in the interests of being open minded, we should also ask:

Question 3. Is this the best approach?

The word “best” is a little subjective, so there is no real definitive answer. However, the somewhat equivocal answer could be “sometimes, yes”, however, of course, this depends on what we are interested in and what we mean by the question. For example if we are interested

in closed geodesics on the surface then these can be viewed dynamically as closed orbits for the geodesic flow. At the same time, in some cases their study can be advanced by other (less dynamical) methods. For example, we note that

1. If V is a compact surface of constant negative curvature there are already powerful techniques (e.g. trace formulae, representation theory) which can often give more precise results.
2. Nevertheless, if V is a non-compact surface of infinite area the above methods may not work so well, but the dynamical approach often still applies. At a certain level this can be thought of as being because the dynamical method uses only the compact recurrent set of the geodesic flow.

Let us now recall a classical example of a compact surface.

Example 1. *Let V be an oriented connected compact surface of genus $g \geq 2$. This surface not only supports a metric of constant curvature $\kappa = -1$, but the space of such metrics is $(6g - 6)$ -dimensional.*

Next we want to consider a couple of examples of infinite area surfaces with constant curvature $\kappa = -1$ to illustrate the second part.

Example 2. *A three funnelled surface, or “a pair of pants”, is a surface homeomorphic to a sphere with three disjoint closed disks removed. It carries metrics with constant negative curvature $\kappa = -1$. We can either consider the complete surface which has three funnels (or ends) or alternatively we can cut along three closed shortest geodesics around each of the funnels to get a surface with three boundary components (as in Figure 2, left). In point of fact, from a dynamical viewpoint the distinction is unimportant. For the geodesic flow on either version the important dynamical component is the recurrent part of the geodesic flow on the 3-dimensional unit tangent bundle. It is a compact set whose intersection with any transverse two-dimensional set is a Cantor set. Since none of the orbits can cross any of the three geodesics around the funnels, the corresponding set appears on the pair of pants.*

Example 3. *A one-holed torus, or a torus with a funnel, is a surface homeomorphic to a torus with a closed disk removed. Similarly to a pair of pants, it carries a metric with constant negative curvature $\kappa = -1$. Again, we can either consider the complete surface which has a single funnel (or end) or alternatively we can cut along the closed geodesic around the funnel to get a surface with a single boundary component (as in Figure 2, right). As in Example 2, from a dynamical viewpoint the distinction is unimportant. The important dynamical component is the recurrent part of the geodesic flow and none of the orbits in the recurrent part can cross the geodesic around the funnel.*

We would like to note that although the approach of Bowen and Series is very successful in the case of surfaces, it does not naturally generalise to higher dimensions.

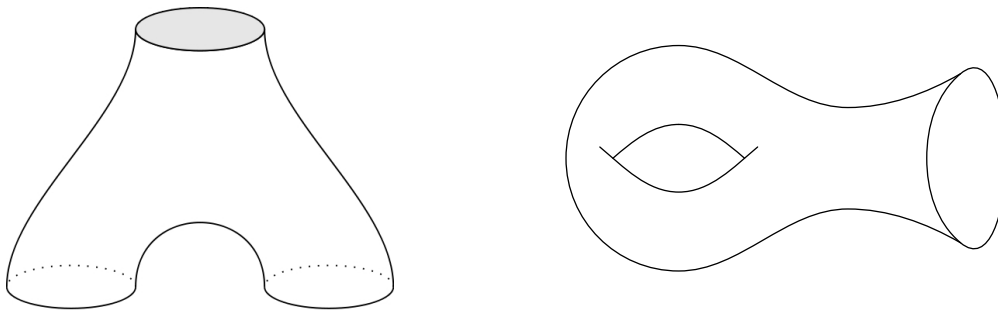


Figure 2: Left: A pair of pants, or a 3-funnelled surface. Right: A one-holed torus or a torus with a funnel. Both drawings represent an artistic impression. According to the Hilbert Theorem, no complete surface of constant negative Gaussian curvature can be isometrically immersed in \mathbb{R}^3 .

3 Hyperbolic Geometry

In this section we want to introduce the setting in which we will be working. This involves recalling some basic definitions and notions in hyperbolic geometry. Hyperbolic geometry was developed in the 19th century by Gauss and Bolyai¹ to show that the 5th postulate of Euclid was not implied by the others.

There are many different models for the hyperbolic space, but we will concentrate on the disk model. We begin with the basic definitions, and refer the reader to the book of Beardon [3] for more details.

Let us denote by $\mathbb{D} = \{z \in \mathbb{C} \mid |z| < 1\}$ the open unit disk in the complex plane.

Definition 1. We can equip \mathbb{D} with the *Poincaré metric* defined locally by

$$ds = \frac{2|dz|}{1 - |z|^2}. \quad (1)$$

In particular, the distance between two points $z_1, z_2 \in \mathbb{D}$ is

$$d(z_1, z_2) = 2 \tanh^{-1} \left| \frac{z_1 - z_2}{1 - z_1 \bar{z}_2} \right|.$$

This defines a complete Riemannian metric on \mathbb{D} . The factor of 2 in the definition of the metric (1) is ensuring a convenient normalisation for the curvature. The Poincaré metric has several useful properties which we briefly summarize below.

Lemma 3. Consider the unit disk equipped with the Poincaré metric (\mathbb{D}, ds) . Then:

1. The space has Gaussian curvature $\kappa = -1$; and

¹This geometry was independently developed by a Russian mathematician N. I. Lobachevski, and carries his name in post-Soviet countries.

2. The orientation preserving isometries take the form of linear fractional transformations

$$g: \mathbb{D} \rightarrow \mathbb{D}; \quad g(z) = \frac{\alpha_1 z + \alpha_2}{\overline{\alpha_2} z + \overline{\alpha_1}}, \quad \text{where } |\alpha_1|^2 - |\alpha_2|^2 = 1, \alpha_1, \alpha_2 \in \mathbb{C}.$$

Note an ambiguity with respect to the simultaneous sign change $(\alpha_1, \alpha_2) \longleftrightarrow (-\alpha_1, -\alpha_2)$ which one has to bear in mind. There are other equivalent models for the hyperbolic plane, such as the Poincaré upper half plane model. However the symmetry of the disk model is particularly useful in what follows in later sections.

For a compact surface V with negative curvature $\kappa = -1$, the Poincaré metric on the unit disk has a particular significance.

Lemma 4. *Let V be a compact surface of constant curvature $\kappa = -1$. Then:*

1. *The Gauss–Bonnet theorem implies that the genus g of V satisfies $g \geq 2$. Equivalently, the Euler characteristic is strictly negative.*
2. *The inequality $g \geq 2$ gives that the universal cover of V is \mathbb{D} and the lifted metric is the Poincaré metric cf. [3].*
3. *The geodesics on V (locally distance minimizing) lift to geodesics on \mathbb{D} . The latter are circular arcs which meet the unit circle $\partial\mathbb{D}$ orthogonally.*

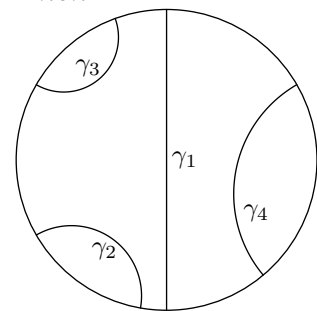


Figure 3: The geodesics in the disk model of the hyperbolic plane.

We have identified in Lemma 3 the group of isometries for the Poincaré metric. We next want to consider its discrete subgroups.

4 Fuchsian groups and the Bowen–Series map

The next ingredient to consider is a suitable subgroup of the isometries of the unit disk with respect to the Poincaré metric. Given a compact surface of constant curvature $\kappa = -1$, we can write $V = \mathbb{D}/\Gamma$ where $\Gamma < \text{Isom}(\mathbb{D}, ds)$ is a discrete subgroup isomorphic to the fundamental group of V , that is $\Gamma = \pi_1(V)$.

4.1 Fuchsian groups

We recall the following standard definition of a Fuchsian group.

Definition 2. We say that $\Gamma < \text{Isom}(\mathbb{D}, ds)$ is a *Fuchsian group* if it is a discrete subgroup.

In other words, $\Gamma < \text{Isom}(\mathbb{D}, ds)$ is Fuchsian, if the orbit $\Gamma 0$ of the point $0 \in \mathbb{D}$ under the action of Γ doesn't have accumulation points inside the disk. Moreover, since $g \in \Gamma$ is a linear

fractional transformation, it can be extended to the boundary $\partial\mathbb{D}$, furthermore, \mathbf{g} preserves the boundary. Hence we can associate to the Fuchsian group Γ an important closed subset of the boundary circle $\partial\mathbb{D}$ called the limit set.

Definition 3. The limit set $\Lambda \subset \partial\mathbb{D}$ consists of Euclidean accumulation points of the orbit of the centre 0, namely,

$$\Lambda = \overline{\Gamma 0} - \Gamma 0.$$

It is not essential to take the orbit of 0; any point in the interior of \mathbb{D} would do. The limit set is always compact. Moreover we know the following:

Lemma 5. *The limit set of a Fuchsian group Γ is either:*

1. *The entire boundary circle, $\Lambda = \partial\mathbb{D}$; or*
2. *A Cantor set of Hausdorff dimension $0 < \delta < 1$.*

These are usually referred to as limit sets of Type I and Type II, respectively.

For the moment, we will focus on the case when $V = \mathbb{D}/\Gamma$ is a compact surface and the associated Fuchsian group Γ is called co-compact. In this case the limit set is the entire circle. The elements of the Fuchsian group Γ have a few useful and important properties.

Lemma 6. *Let $V = \mathbb{D}/\Gamma$ be a compact connected surface of constant negative curvature and genus g .*

1. *Every transformation $\mathbf{g} \in \Gamma \setminus \{e\}$ has two fixed points, a repelling and an attracting one, on $\partial\mathbb{D}$. We denote the attracting point by $p_{\mathbf{g}}^+$, so that $|\mathbf{g}'(p_{\mathbf{g}}^+)| < 1$. Similarly, we let $p_{\mathbf{g}}^-$ denote the repelling point, so that $|\mathbf{g}'(p_{\mathbf{g}}^-)| > 1$.*
2. *The group Γ is finitely generated and finitely presented. For instance, there exists a finite set of generators $a_j \in \Gamma$, $j = 1, \dots, 2g$ such that*

$$\Gamma = \langle a_1, a_2, \dots, a_{2g} \mid (a_1 a_2^{-1} a_3 a_4^{-1} \dots a_{2g-1} a_{2g}^{-1}) \cdot (a_1^{-1} a_2 a_3^{-1} a_4 \dots a_{2g-1}^{-1} a_{2g}) = 1 \rangle.$$

4.2 Bowen–Series map

Given a Fuchsian group we want to define a piecewise continuous expanding Markov map called the *Bowen–Series map* defined on the boundary $\partial\mathbb{D}$.

In order to define the map $T: \partial\mathbb{D} \rightarrow \partial\mathbb{D}$ we need to define a partition of the boundary. The construction below relies on Ford fundamental domain.

To every $\mathbf{g} \in \Gamma$ we relate an *isometric circle*:

$$C(\mathbf{g}) = \{z \in \mathbb{D} \mid |\mathbf{g}'(z)| = 1\}$$

The name isometric here refers to the fact that \mathbf{g} locally doesn't change Euclidean length. A nice treatment of isometric circles can be found in Ford's monograph [16].

The isometric circle of an isometry $C(\mathbf{g})$ is a geodesic in the Poincaré metric. Indeed, assuming $\mathbf{g}(z) = \frac{\alpha_1 z + \alpha_2}{\alpha_2 z + \alpha_1}$ we get $\mathbf{g}'(z) = (\alpha_2 z + \alpha_1)^{-2}$. Therefore $|\mathbf{g}'(z)| = 1$ defines a circle of radius $|\alpha_2|^{-1}$ centred at $-\overline{\alpha_1}/\overline{\alpha_2}$ provided $\alpha_2 \neq 0$. To see that it is a geodesic, observe that the triangle with vertices at the origin, the centre of $C(\mathbf{g})$, and a point of the intersection of $C(\mathbf{g})$ and $\partial\mathbb{D}$ is right-angled. A useful property is that a map $\mathbf{g} \in \Gamma$ transfers its isometric circle to the isometric circle of its inverse: $\mathbf{g}C(\mathbf{g}) = C(\mathbf{g}^{-1})$.

The region of the unit disk “exterior” to the isometric circles of *all* elements of Γ is a fundamental domain for the Fuchsian group Γ . It is called *Ford domain*. It is known that every side s of the fundamental domain is identified with another one by an element of Γ that we shall denote $\mathbf{g}(s)$. Moreover,

$$\Gamma = \langle \mathbf{g}(s) \mid s \text{ is a side of the Ford fundamental domain of } \Gamma \rangle,$$

in other words, the elements identifying the sides of the Ford domain constitute a set of generators of Γ .

In order to guarantee that the boundary map we are about to define is Markov, we need to impose additional assumptions on the way the surface group acts on the hyperbolic plane:

- Every side s of a fundamental domain lies on the isometric circle of $\mathbf{g}(s)$, i.e. $s \subset C(\mathbf{g}(s))$;
- All hyperbolic lines, containing sides of the fundamental domain, are entirely covered by images of the sides of the fundamental domain under action of Γ .

Remark 1. In many cases the assumption may not hold, but then there exists another representation of the fundamental group $\Gamma = \pi_1(V)$ for which this property holds. The choice of Γ was written down independently by both Bowen–Series [7] and Adler–Flatto [2]. In the interests of clarity and historical reverence we will use the original construction of Bowen and Series [7].

Under the above assumptions, configuration of the isometric circles takes the form illustrated in Figure 3, adapted from [7, Fig. 3]. The boundary of the fundamental domain is given by arcs of isometric circles of generators of Γ . Each of the circles may intersect with its direct neighbours, but no more. Their endpoints give a partition of the boundary. We can now pick every second point and use these points on the boundary circle to divide it into the same number of arcs, and then define an analytic map to each of these arcs.

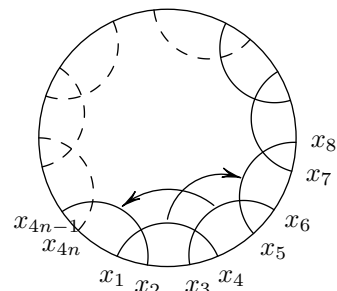


Figure 3: Isometric circles.

This will give us a required map of the circle, that we treat as an interval with endpoints identified, and the arcs are thought of as intervals, in the usual way. More precisely, we enumerate the sides of the fundamental domain as s_1, \dots, s_{2n} in anti-clockwise direction and denote the

end points of the isometric circle corresponding to s_j by x_{2j-1} and x_{2j+2} , for $j = 1, \dots, 2n - 1$, and the end points of s_{2n} we label x_{4n-1} and x_2 . Then we define $T: \partial\mathbb{D} \rightarrow \partial\mathbb{D}$ by

$$T(x) = \begin{cases} \mathbf{g}(s_j)(x), & \text{if } x \in [x_{2j-1}, x_{2j+1}), \text{ for some } j < 2n; \\ \mathbf{g}(s_{2n})(x), & \text{if } x \in [x_{4n-1}, x_1). \end{cases} \quad (2)$$

We summarise the main properties of the map T in the following lemma.

Lemma 7. *The interval map T is:*

1. *Real analytic on each interval of the partition specified in (2);*
2. *Uniformly expanding: $\exists \beta > 1$ such that $|T'(z)| \geq \beta$ for every $z \in \partial\mathbb{D}$;*
3. *Markov: there exists a finite refinement of the partition described in (2) with respect to which T has Markov property. More precisely, one needs to take the endpoints of all sides of the tessellation that go through the vertices of the fundamental domain. The assumptions on the action of Γ guarantee the finiteness of the refined partition.*

These properties are very classical and lead to a clear understanding of the dynamics of the map. Moreover, these can be used to understand the induced action of the Fuchsian group Γ on the boundary. In particular, we would like to replace the action

$$\Gamma \times \partial\mathbb{D} \rightarrow \partial\mathbb{D} \quad (\mathbf{g}, x) \mapsto \mathbf{g}(x)$$

by a single transformation $T: \partial\mathbb{D} \rightarrow \partial\mathbb{D}$ (up to finitely many points, which are the end points of the isometric circles).

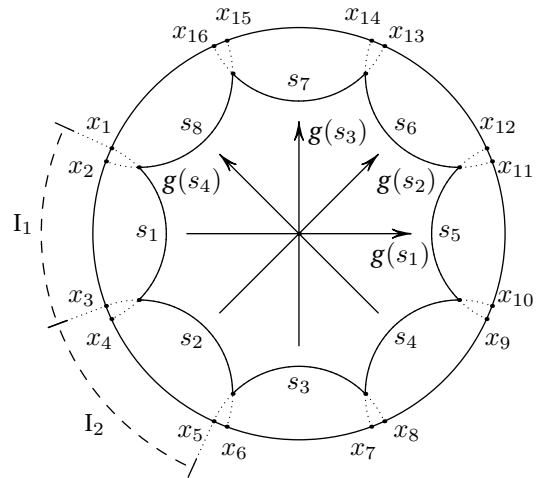
Let us denote by Γx the orbit of x under the action of the group, i.e., $\Gamma x = \{\mathbf{g}x \mid \mathbf{g} \in \Gamma\}$.

Lemma 8. *The orbit Γx of a typical point $x \in \partial\mathbb{D}$ can be written as an equivalence class*

$$\Gamma x = \{y \mid \exists n, m \geq 0: T^n x = T^m y\},$$

where T is defined by (2).

Example 4. *Consider a regular hyperbolic octagon with angles $\frac{\pi}{4}$. We can enumerate the edges s_j , $j = 1, \dots, 8$. Then we may consider the orientation preserving isometries Γ_0 of the hyperbolic plane which identify the opposite sides. Let Γ be the group generated by Γ_0 . One can check that the octagon is the fundamental domain of Γ and s_i is isometric circle of $\mathbf{g}(s_i)$. It follows by the symmetry that the Bowen–Series map T has 16 arcs of continuity, all of the same length. We would like to stress that T is not Markov with respect to this partition, one needs to refine it. (See figure on the right, corresponding to the case when $V = \mathbb{D}/\Gamma$ is the Bolza surface.)*



5 Dynamical Applications: Compact surfaces

We now return to the study of the dynamical properties of the geodesic flows on surfaces, particularly those which can be approached from the perspective of the associated Bowen–Series map on the unit circle (or more accurately, on a disjoint union of intervals). We would like to highlight two particularly well known properties.

5.1 Counting closed geodesics

We begin with a topological result. Let V be a compact surface of constant negative curvature. It is easy to see that there are infinitely many closed geodesics since each free homotopy class (i.e., conjugacy class) in $\pi_1(V)$ contains a closed geodesic. Furthermore, there are countably many closed geodesics since each free homotopy class for a negatively curved surface contains precisely one closed geodesic. By a closed geodesic we mean the directed closed geodesics, i.e., each curve considered as a set actually corresponds to two directed geodesics, which differ by orientation.

Let us denote by $\ell(\gamma)$ the length a (primitive) closed geodesic γ . Closed geodesics are in bijection with the (prime) closed orbits of the geodesics flow of the same length.

Notation. *The number of closed geodesics whose length is at most t we denote by*

$$N(t) := \#\{\gamma \text{ is primitive closed geodesic and } \ell(\gamma) \leq t\}$$

It is well known that $N(t)$ is finite [9, Ch 9, §2]. Let us recall the further properties.

Lemma 9. *For a compact negatively curved surface we have:*

1. $N(t)$ is monotone increasing; and

2. $\lim_{t \rightarrow \infty} \frac{1}{t} \log N(t) = 1$.

The quantity that appears in the second part is the topological entropy of the geodesic flow. A much stronger result than Part (2) of Lemma 9 is the following asymptotic.

Theorem 1 (Huber [20, Satz 9]). *Let V be a compact surface of constant negative curvature -1 . Then*

$$\lim_{t \rightarrow \infty} \frac{N(t)}{e^t} \cdot t = 1.$$

The natural proof of Huber’s theorem uses the Selberg zeta function $Z_V(s)$ and the location of its zeros. We recall the definition.

Definition 4. We formally define the Selberg zeta function as an infinite product

$$Z_V(s) = \prod_{n=0}^{\infty} \prod_{\gamma} (1 - e^{-(s+n)\ell(\gamma)}), \quad s \in \mathbb{C}, \quad (3)$$

where the product is taken over all closed geodesics on V and $\ell(\gamma)$ stands for the length of γ . The function is well defined, as the product converges to an analytic function for $\Re(s) > 1$.

The convergence of the infinite product from (3) on $\Re(s) > 1$ follows from the estimate in Lemma 9. The asymptotic estimates for the counting function $N(t)$ follow completely by analogy with the Prime Number Theorem for primes and the zeta function $Z_V(s)$ is used in place of the Riemann ζ -function.

The zeta function $Z_V(s)$ formally defined on $\Re(s) > 1$ can be extended to the entire complex plane using the famous Selberg trace formula [24]. This is explained in the book of Hejhal [19] in considerable detail. We recall the basic properties:

Lemma 10. *Let V be a compact surface of constant negative curvature. Then the Selberg zeta function has the following properties:*

1. $Z_V(s)$ analytic and non-zero for $\Re(s) > 1$;
2. $Z_V(s)$ has a simple zero at $s = 1$;
3. $Z_V(s)$ has an analytic extension to \mathbb{C} .

Remark 2. Margulis [22] gave a generalisation of Huber’s theorem to the case of surfaces of variable negative curvature in his 1972 PhD thesis, that was published in English more than 30 years later. Margulis’ approach to Huber’s theorem (for $\kappa < 0$) uses strong mixing of a suitable invariant measure (nowadays called the Bowen–Margulis measure) which maximises the entropy. The approach introduced by Margulis has now been adapted to a number of interesting generalizations.

We want to consider error terms in the asymptotic relation from Theorem 1. To put this into perspective we need to recall what might happen in the corresponding setting in number theory.

5.2 Taking a leaf out of the number theory book

Let us begin by recalling some classical ideas from number theory. These are useful in understanding the role of the dynamical analogues.

Riemann ζ -function. We recall the definition of the Riemann ζ -function:

$$\zeta(s) = \sum_{n=1}^{\infty} \frac{1}{n^s} = \prod_p (1 - p^{-s})^{-1}$$

where the Euler product is over the prime numbers. Below are some of the properties of this famous function.

Lemma 11. *The Riemann zeta ζ function has the following properties:*

1. $\zeta(s)$ is analytic and non-zero for $\Re(s) > 1$;

2. $\zeta(s)$ has a simple pole at $s = 1$;
3. $\zeta(s)$ has analytic extension to $\mathbb{C} \setminus \{1\}$.

Of course there is additionally another property which has not yet been established.

Riemann hypothesis (1859): All zeros of ζ in semi-plane $\Re(s) > 0$ lie on a line $\Re(s) = \frac{1}{2}$.

This question is also known as Hilbert’s 8’t h Problem and a Clay Institute Millennium Problem. There have been many attempts to prove this result, but so far the conjecture has resisted attempts. One particularly popular approach is the following:

Hilbert–Polya approach: Try to relate the zeros of ζ to eigenvalues of some self-adjoint operator.

The motivation for this idea is the fact that the spectrum of a self-adjoint operator is necessarily contained in \mathbb{R} . Whereas it has proved elusive for the Riemann zeta function, the analogue for the Selberg zeta function has been more successful.

5.3 Error terms in counting closed geodesics

There is an improvement to Huber’s basic Theorem 1 at least as stated. In fact, the original result of Huber included error terms, so now we are actually stating more of his original theorem.

Theorem 2 (Huber [21, Satz IV]). *Let V be a compact surface with constant gaussian curvature $\kappa = -1$. There exists $\varepsilon > 0$ such that*

$$N(t) = \int_2^{e^t} \frac{1}{\log u} du (1 + O(e^{-\varepsilon t})) = \text{li}(e^t) (1 + o(e^{-\varepsilon t})) \quad \text{as } t \rightarrow +\infty.$$

In other words, there exist $\varepsilon > 0$ and $C > 0$ such that $\left| \frac{N(t)}{\text{li}(e^t)} - 1 \right| \leq C e^{-\varepsilon t}$.

Note that ε here is responsible for the rate of convergence, rather than “just” for the error term itself.

As is well known,

$$\text{li}(x) := \int_2^x \frac{du}{\log u} \sim \frac{x}{\log x} \text{ as } x \rightarrow +\infty.$$

Therefore this statement is consistent with the original statement of Theorem 1, but now has an additional error term.

The proof uses properties of Z_V and the rate $\varepsilon > 0$ depends on location of zeros. This is completely analogous to the situation in number theory where one studies a counting problem for prime numbers by using the Riemann zeta function, except in the present context we have stronger results on the zeta function.

For compact surfaces there is a natural self-adjoint operator. The extension and zeros of Selberg zeta function are related to *the Laplacian* $\Delta: \mathcal{L}^2(V) \rightarrow \mathcal{L}^2(V)$. This can be defined as an operator on real analytic functions $\Delta: C^\omega(V) \rightarrow C^\omega(V)$ and then extended to square integrable functions. Let

$$\Delta\psi_n + \lambda_n\psi_n = 0$$

be the eigenvalue equation. There are infinitely many eigenvalues

$$0 = \lambda_0 < \lambda_1 \leq \lambda_2 \leq \dots \nearrow +\infty$$

for the operator $-\Delta$. Moreover, we have the following results:

1. $\#\{\lambda_n \leq t\} \sim \frac{\text{Area}(V)}{4\pi} \cdot t$ as $t \rightarrow \infty$ (Weyl, 1911);
2. The zeros of $Z_V(s)$ in $0 < \Re(s) < 1$ satisfy the equality $s_n(1 - s_n) = \lambda_n$, where λ_n are eigenvalues of the Laplacian [37].

The second statement implies that $s_n = \frac{1}{2} \pm \sqrt{\frac{1}{4} - \lambda_n}$, and lie on $[0, 1] \cup \{\Re(s) = \frac{1}{2}\}$. This can be thought of as an analogue of the ‘‘Riemann Hypothesis’’. We can formulate it as follows:

Corollary 1. *Let V be a compact surface and let s_n be a zero of the associated Selberg zeta function Z_V defined by (3). Then either $s_n \in [0, 1]$ or $\Re(s_n) = \frac{1}{2}$.*

The proof uses trace formulae to relate the zeros of Z_V to the eigenvalues of the Laplacian. It is the self-adjointness of the Laplacian which ultimately leads to this property.

The parameter $\varepsilon > 0$ for the error term for counting closed orbits in Theorem 2 can be expressed in terms of the eigenvalues of the Laplacian, namely, it corresponds to the distance of the zeros of Z_V from the line $\Re(s) = 1$ (although one may need to take ε slightly smaller).

Remark 3. The value of $\varepsilon > 0$ can be arbitrary small. This follows from its spectral interpretation (in terms of the Laplacian) and corresponds to having eigenvalues close to 0. Using classical results of Cheeger [11], Schoen–Wolpert–Yau [36] one can show that $\varepsilon \asymp \ell(\gamma_0)$ where $\ell(\gamma_0)$ is the length of the shortest closed dividing geodesic on V .

The approach and the statement fail if V has infinite area. In general case there is no reason for zeros to lie on such lines. In the context of non-compact surfaces we need an alternative approach using the Bowen–Series map, that allows us to establish a correspondence between closed geodesics and closed orbits.

Recall that a geodesic is called prime if it traces its path exactly once. We say that a periodic orbit $\{x, Tx, \dots, T^{n-1}x \mid T^n x = x\}$ is prime if $T^k x \neq x$ for all $1 \leq k < n$.

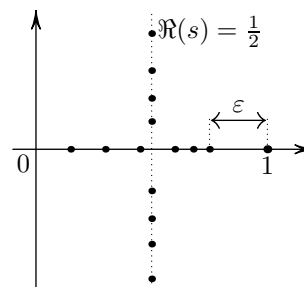


Figure 4: The zeros of the Selberg zeta function

Lemma 12. *There is a bijection between closed (prime) geodesics γ on V and closed (prime) orbits $\{x, Tx, \dots, T^{n-1}x \mid T^n x = x\}$, where T is defined by (2), except for a finite number of geodesics corresponding to the endpoints of the intervals of analyticity of T .*

An advantage of the Bowen–Series construction is that the map T defined by (2) can be used to recover the lengths of closed geodesics. More precisely,

Lemma 13. *If γ is a prime closed geodesic of length $\ell(\gamma)$ with associated prime periodic T -orbit*

$$\{x, Tx, \dots, T^{n-1}x \mid T^n x = x\},$$

then $\ell(\gamma) = \log |(T^n)'(x)|$.

In particular, we can interpret the length of γ as the Lyapunov exponent of the periodic orbit, which gives a clue to the Lemma.

To take advantage of this correspondence to study zeta function Z_V , we introduce the family of complex Ruelle–Perron–Frobenius transfer operators (indexed by $s \in \mathbb{C}$). This is often referred to as the “Thermodynamic Viewpoint” [30]. We begin by recalling the definition.

Definition 5. Given a (possibly infinite) disjoint union of intervals X and associated piece-wise analytic map T we can define a family of *transfer operators* on a space of continuous functions $\mathcal{L}_s: C^0(X) \rightarrow C^0(X)$ by

$$[\mathcal{L}_s f](x) = \sum_{Ty=x} e^{-s \log |T'(y)|} f(y), \quad s \in \mathbb{C}$$

Remark 4. When $s = 1$, this reduces to the “usual” Ruelle–Perron–Frobenius operator for an expanding interval map.

However, in order to proceed we need to replace the big space $C^0(X)$ by a smaller Banach space upon which the transfer operator has good spectral estimates.

5.4 The Banach spaces

Let $\{I_j\}$ denote the arcs in the Bowen–Series coding (not to be confused with intervals from the definition of T).

1. Choose (small) open neighbourhoods $I_j \subset U_j \subset \mathbb{C}$ such that for any $I_j \subset T(I_k)$ we have that the closure $\overline{U_j} \subset T(U_k)$;
2. Let $B \subset C^0(\bigsqcup_k U_k)$ be the Banach space of bounded analytic functions on the disjoint union $\bigsqcup_k U_k$ with the supremum norm

$$\|f\| = \sup_{z \in \bigsqcup_k U_k} |f(z)|;$$

3. By construction we see that the Banach space is preserved by all \mathcal{L}_s , i.e., $\mathcal{L}_s: B \rightarrow B$ for all $s \in \mathbb{C}$;

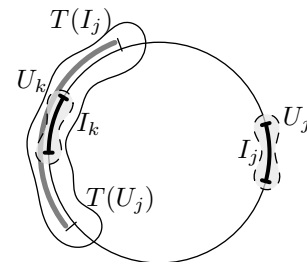


Figure 5: Arcs $I_j \subset \partial\mathbb{D}$ of a Markov partition of T , their images and neighbourhoods.

4. On the Banach space B we have that \mathcal{L}_s is trace class; in other words, there exists only countable many non-zero eigenvalues and their sum is finite². The finiteness of trace allows us to write

$$\det(I - \mathcal{L}_s) := \exp\left(-\sum_{n=1}^{\infty} \frac{1}{n} \text{trace}(\mathcal{L}_s^n)\right),$$

where the right hand side converges to an analytic function for all $s \in \mathbb{C}$; and

5. Furthermore the connection between the derivative of T and the length of closed geodesics allows one to establish $Z_V(s) = \det(I - \mathcal{L}_s)$; Finally
6. We have the classical observation: $Z_V(s) = 0$ if and only if there exists a non-zero function $f \in C^\omega(\sqcup_k U_k)$ such that $\mathcal{L}_s f = f$.

We will return to the use of Banach spaces later in the special case of infinite area surfaces, where the compactness enters via the limit set Λ .

5.5 Mixing of geodesic flow

We next consider a closely related problem in the general area of smooth ergodic theory. We begin with a definition.

Definition 6. Let Y be the unit tangent bundle to a surface V and let ν be a (normalised) Liouville measure on Y . Given two smooth functions $F, G: Y \rightarrow \mathbb{R}$ and a geodesic flow φ_t on Y , we define a correlation function:

$$\rho(t) = \int_Y F(\varphi_t x) G(x) d\nu(x) - \int_Y F d\nu \int_Y G d\nu, \quad t \geq 0,$$

We say that the flow is strong mixing if $\rho(t) \rightarrow 0$ as $t \rightarrow +\infty$. The rate of convergence in this case is referred to as *the rate of mixing*.

In the case of constant negative curvature the Liouville measure corresponds to the normalised Haar measure.

Mixing is a property in the hierarchy of ergodic properties. It implies ergodicity and is in turn implied by the Bernoulli property. In the case of square integrable functions $F, G \in L^2(\nu)$ there is no reason to expect to be able to say anything about the speed of mixing (i.e., the rate at which $\rho(t)$ tends to zero). But since we are assuming F and G are smooth more can be said.

Of course the definition can also be reformulated for different invariant measures, but for our present purposes we only need to consider the measure ν .

The following result dates back over sixty years and was the forerunner of method that has proved to be very successful over subsequent years.

²This follows directly from the fundamental work of Grothendieck [17], [18] and Ruelle [35]. We also refer the reader to [23].

Theorem 3 (Fomin–Gelfand, 1952). *The geodesic flow on a manifold of constant negative curvature, is strong mixing, in other words $\rho(t) \rightarrow 0$ as $t \rightarrow +\infty$.*

The proof of Theorem 3 uses unitary representation of $SL(2, \mathbb{R})$ on the space $L^2(Y)$ given by $[U_g f](x) = f(\mathbf{g}^{-1}x)$. The representation U_g is reducible and therefore the problem of establishing strong mixing is reduced to the understanding of the action of each of the component representations. This brings us to the next question:

Question 4. Can we estimate the speed of convergence $\rho(t) \rightarrow 0$ or improve on these results in any way?

The following results on mixing don't directly rely on properties of the zeta function, but the underlying mechanisms are similar as will hopefully soon become apparent.

Theorem 4. *Let V be a compact surface of constant curvature $\kappa = -1$ and let Y be its unit tangent bundle. Given two functions $F, G \in C^\infty(Y)$ there exist $\varepsilon > 0$, $C > 0$ such that the correlation function of the geodesic flow φ_t satisfies*

$$|\rho(t)| \leq C e^{-\varepsilon t}, \quad t \geq 0,$$

where C depends on F and G , but ε depends only on the geodesic flow.

The argument is based on representation theory approach. In fact the correlation functions correspond to “decay of matrix coefficients” in representation theory [26].

We have used the same constant $\varepsilon > 0$ for both results, in the counting geodesics problem Theorem 2, and for the speed of mixing of geodesic flow in Theorem 4. Assuming this wasn't carelessness, one might ask the following question:

Question 5. How are the ε 's related in two problems?

The simple answer is: “*They are the same!*”. To see this, we can consider the Laplace transform of the correlation function ρ :

$$\hat{\rho}(z) = \int_0^\infty e^{-zt} \rho(t) dt, \quad z \in \mathbb{C}.$$

Thus we are introducing another complex function to describe the mixing rate. The function $\hat{\rho}$ is well-defined for $\Re(z) > 0$ since the integral converges on this half-plane. However, there is much more that one can say. We recall the following properties of $\hat{\rho}$.

Lemma 14. *The Laplace transform of the correlation function has the following properties:*

1. *The function $\hat{\rho}$ extends meromorphically to \mathbb{C} ;*
2. *Poles z_n for $\hat{\rho}$ are related to zeros s_n for the zeta function Z_V by $z_n = s_n - 1$; and*

3. The absence of poles for the Laplace transform $\hat{\rho}$ for a large half-plane $\Re(z) > -\varepsilon$ implies exponential decay of ρ (here ε is the same as in Theorem 4).

The existence of meromorphic extension of $\hat{\rho}$ can be obtained by establishing a connection with the resolvent of the transfer operators and using properties of the spectrum of the transfer operator. The second part follows from the observation that Z_V has a similar connection to the spectra of a suitable transfer operator. The last part is classical harmonic analysis using the Paley–Wiener theorem.

Definition 7. The poles of the meromorphic extension of $\hat{\rho}$ (or sometimes zeros of Z_V) are called *resonances*.

6 The Bowen–Series map for infinite area surfaces

Henceforth, we now want to consider the case of infinite area surfaces V . However, we shall only consider the case that V has no cusps, or equivalently the corresponding Fuchsian group Γ has no parabolic points.

We want to construct the boundary map associated to the action of the group on the limit set. Recall that by Lemma 5 in this case the limit set Λ is a Cantor set. The same basic approach applies — except that it is even easier: this time we have to define an expanding map $T: \Lambda \rightarrow \Lambda$ on the Cantor set. This is best illustrated by an example. We recall our basic example of the three funnelled surface.

Example 5 (Three funnelled surface). *Let V be the three funnelled surface described in Example 2. We can write $V = \mathbb{D}/\Gamma$ where $\Gamma = \pi_1(V)$ is the associated Schottky group of isometries. Since V homotopically equivalent to figure eight, $\Gamma = \langle \mathbf{g}_1, \mathbf{g}_2 \rangle$ as a free group on two generators $\mathbf{g}_1, \mathbf{g}_2 \in \text{Isom}(\mathbb{D})$. One classical construction is to take two pairs of disjoint geodesics $\gamma_0, \gamma_1, \gamma_2, \gamma_3$ and isometries identifying geodesics within each pair and mapping “exterior” of γ_j into “interior” of $\gamma_{(j+2)\bmod 4}$, as pictured in Figure 6, so that $\mathbf{g}_0: \gamma_0 \rightarrow \gamma_2$, $\mathbf{g}_1: \gamma_1 \rightarrow \gamma_3$, and $\mathbf{g}_2 = \mathbf{g}_0^{-1}$, $\mathbf{g}_3 = \mathbf{g}_1^{-1}$. Let Λ_j be the part of Λ enclosed between the end points of γ_j . Thus we have a partition $\Lambda = \sqcup_j \Lambda_j$.*

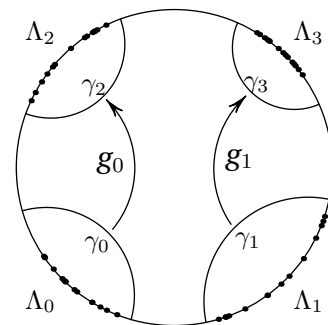


Figure 6: Partition of the Cantor set $\sqcup_j \Lambda_j$.

We can then define a Bowen–Series map $T: \Lambda \rightarrow \Lambda$ by $T(x) = \mathbf{g}_j(x)$ for $x \in \Lambda_j$. It is easy to see that this is strictly expanding (i.e., $|T'(x)| > 1$ for $x \in \Lambda$) and Markov, in the sense that the image $T(\Lambda_j)$ is the union of the three elements of the partition

$$\Lambda_j = \bigcup_{k \neq (j+2)\bmod 4} \Lambda_k.$$

In Lemma 5 we introduced Hausdorff dimension δ of the limit $\Lambda \subset \partial\mathbb{D}$. It turns out we can write δ in terms of the transformation $T: \Lambda \rightarrow \Lambda$ and its derivative. In order to formulate this we need the following definition of a pressure functional.

Definition 8. We define the *pressure functional* $P : C^0(\Lambda) \rightarrow \mathbb{R}$ by

$$P(f) := \lim_{n \rightarrow \infty} \frac{1}{n} \log \left(\sum_{T^n x = x} \exp \left(\sum_{j=0}^{n-1} f(T^j x) \right) \right).$$

Equivalently, we can define the pressure using the variational principle:

$$P(f) := \sup \left\{ h_{\text{top}}(\mu) + \int f d\mu \mid \mu \text{ is a } T\text{-invariant probability measure.} \right\}$$

It is a classical result that in the present context of expanding maps the limit always exists and finite, we refer the reader to [30] for details. We now have the following promised characterisation of $\delta = \dim_H \Lambda$ in terms of the functions on the boundary.

Lemma 15. *The Hausdorff dimension $\delta = \dim_H \Lambda$ satisfies $P(-\delta \log |T'(x)|) = 0$.*

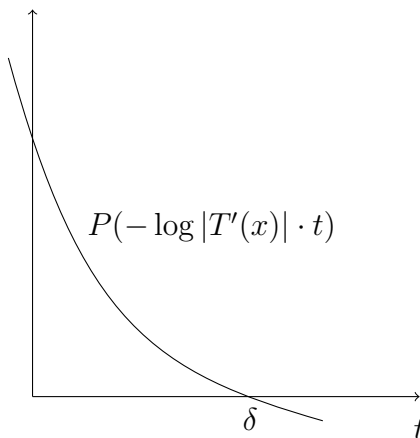


Figure 7: A typical plot of the pressure function.

By analogy with the case of compact surfaces, we can introduce a family of complex Ruelle–Perron–Frobenius transfer operators ($s \in \mathbb{C}$) initially defined on continuous³ functions $C^0(\Lambda)$ on the limit set Λ .

Definition 9. We can define the *transfer operators* $\mathcal{L}_s : C^0(\Lambda) \rightarrow C^0(\Lambda)$ by

$$\mathcal{L}_s f(x) = \sum_{Ty=x} e^{-s \log |T'(y)|} f(y), \quad s \in \mathbb{C}. \quad (4)$$

This gives us another interpretation of the value $\delta = \dim_H \Lambda$.

Lemma 16. *The parameter value $s = \delta$ corresponds to the case when the operator \mathcal{L}_s has the maximal eigenvalue 1.*

As before, to study the zeta function Z_V using the transfer operators we need to replace $C^0(\Lambda)$ by a smaller Banach space upon which the transfer operator has good spectral estimates.

³in the induced topology on $\partial\mathbb{D}$.

7 Dynamical applications: non-compact surfaces

We want to find analogues of the counting and mixing results from Theorems 2 and 4, respectively, in the case that we have a surface of infinite area. We begin with the counting problem for closed geodesics.

7.1 Counting closed geodesics

As in the case of compact surfaces, one has in the non-compact case that there are infinitely many closed geodesics (with one in each free homotopy class). The obvious question is the following.

Question 6. What are the analogous results on the asymptotic behaviour of the number of closed geodesics in non-compact case?

Assume that $V = \mathbb{D}/\Gamma$ is a surface of infinite area, where Γ denotes the associated Fuchsian group. We first recall that δ denotes the Hausdorff dimension of the limit set and let us again denote by $\#\{\gamma: \ell(\gamma) \leq t\} =: N(t)$ the number of prime closed geodesics of length at most t . Now we can state the first result, which gives that δ is also the asymptotic growth rate of $N(t)$.

Lemma 17. *The value $\delta = \dim_H \Lambda$ is the growth rate of the number of closed geodesics:*

$$\delta = \lim_{t \rightarrow \infty} \frac{1}{t} \log \#\{\text{prime closed geodesic } \gamma \text{ with } \ell(\gamma) \leq t\}.$$

The stronger asymptotic result in the case of closed geodesics for compact surfaces (Theorem 1) can also be extended to this case.

Theorem 5. *We can write*

$$N(t) \sim \frac{e^{\delta t}}{\delta t} \text{ as } t \rightarrow +\infty$$

(Compare with the compact case result in Theorem 1 taking into account that in that case the limit set is the entire circle and $\delta = 1$.)

However, whereas the proof in the case of compact surfaces used the Selberg trace formulae this is not available to us in the case of general infinite area surfaces. Instead in the present setting the transfer operators can be used to give an extension to the zeta function Z_V and this leads to a proof of Theorem 5. Similarly to the compact case there is a stronger form of the asymptotic formula with an error term.

Theorem 6 (Naud 2005). *There exists $\varepsilon > 0$ such that*

$$N(t) = \int_2^{e^{\delta t}} \frac{1}{\log u} du (1 + O(e^{-\varepsilon t})) = \text{li}(e^{\delta t}) + O(e^{(\delta-\varepsilon)t}), \text{ as } t \rightarrow +\infty.$$

Both results Theorem 6 and Theorem 5 require the dynamical approach of transfer operators. This method also applicable in the case of compact surfaces, but in that case we had the luxury of using the trace formulae, which served us even better in as much as they gave both an analytic extension and additional information on the location of the zeros. Despite its apparent greater generality, or perhaps because of it, the transfer operator approach has the downside that there is less control over the location of zeros. The next lemma is the analogue of Lemma 12 for compact surfaces.

Lemma 18. *There is a one-to-one correspondence between*

1. *Closed (prime) geodesics γ ; and*
2. *Periodic (prime) orbits of the Bowen–Series map $\{x, Tx, \dots, T^{n-1}x\}$ where $T^n x = x$.*

In fact, Lemma 18 has one improvement on Lemma 12 in as much as there is a bijection, without having to concern ourselves with a finite number of exceptional geodesics.

As in the case of compact surfaces we have the following correspondence for the lengths (compare with Lemma 13).

Lemma 19. *To every prime closed geodesics γ which is not a bounding curve we can associate a periodic (prime) orbit of a Bowen–Series map $\{x, Tx, \dots, T^{n-1}x\}$, $T^n x = x$ where $\ell(\gamma) = \log |(T^n)'(x)|$.*

We again define the Selberg zeta function

$$Z_V(s) = \prod_{n=0}^{\infty} \prod_{\gamma} (1 - e^{-(s+n)\ell(\gamma)}) \quad (5)$$

where the product is taken over all prime closed geodesics γ and $\ell(\gamma)$ is the length; as before in (3). Note that in the case of infinite area surfaces the closed geodesics are contained in the *recurrent* part of the flow. The infinite product on the right hand side of (5) converges for $\Re(s) > \delta$ as is easily seen using Theorem 5 and defines an analytic function.

To proceed we again replace $C^0(X)$ by a smaller Banach space upon which the transfer operator has good spectral estimates (e.g. Hölder, C^1 , C^k , C^ω , the smaller space the better the results).

7.2 The Banach spaces

The main case we want to concentrate on is the three funnelled surface (or “pair of pants”) from Example 5. This will be a paradigm for a general case.

In order to study the zeta function Z_V using the transfer operator we need to be more restrictive in the type of Banach space upon which the transfer operator acts. We will consider a Banach space of analytic functions.

1. Choose four disjoint open neighbourhoods $U_j \supset \Lambda_j$ of elements of partition of the Cantor set, as pictured in Figure 6;
2. Let $B \subset C^\omega(\sqcup_j U_j)$ be the *Banach space* of bounded analytic functions on the disjoint union of the disks $\sqcup_j U_j$ with the norm

$$\|f\| = \sup_{z \in \sqcup_j U_j} |f(z)|.$$

Of course, this is equivalent to the direct sum of spaces of analytic functions on each of the four neighbourhoods.

3. By construction we see that the Banach space is preserved by transfer operators given by (4), i.e., $\mathcal{L}_s: B \rightarrow B$ for every $s \in \mathbb{C}$.
4. On the Banach space B we have that \mathcal{L}_s is trace class, in particular, there exists only a countable set of non-zero eigenvalues which sum is finite⁴. Thus we can write

$$\det(I - \mathcal{L}_s) := \exp \left(- \sum_{n=1}^{\infty} \frac{1}{n} \text{trace}(\mathcal{L}_s^n) \right)$$

and the right hand side converges to a function analytic on \mathbb{C} .

5. Furthermore using the connection between the derivatives of the Bowen–Series map and closed geodesics one can show that $Z_V(s) = \det(I - \mathcal{L}_s)$.
6. Finally, we have the classical observation: $Z_V(s) = 0$ if and only if there exists a function $f \neq 0 \in B$ such that $\mathcal{L}_s f = f$. Thus in order to show that there is a zero free strip it suffices to show that there exists $\delta' < \delta$ such that for any $\delta' < \Re(s) < \delta$ the operator \mathcal{L}_s doesn't have 1 as an eigenvalue.

As we have observed already, closed geodesics in the case of non-compact surfaces lie in the recurrent part of the geodesic flow. We also adopt the convention that they are oriented geodesics (i.e., a pair of geodesics which are identical as sets but have different orientations counted as two different geodesics).

We recall basic properties of the zeta function (cf. [31]) for infinite area surfaces.

Lemma 20. *Let V be an infinite area surface of constant negative Gaussian curvature -1 .*

1. *The infinite product (5) converges for $\Re(s) > \delta$ and therefore Z_V is a well defined analytic function on this half-plane;*
2. *The zeta function Z_V has an analytic extension to \mathbb{C} .*

⁴This again follows directly from the works of Grothendieck [17], [18] and Ruelle [35].

7.3 Measures and mixing

To extend the theory to the case of surfaces of infinite area we first need a new measure replacing the Haar measure. In this case we are concerned with measures supported on the recurrent part of the geodesic flow. The easiest way to construct such measures is by using the classical construction of measures on the limit set and then to convert these into measures invariant by the geodesic flow and supported on the recurrent part of the flow.

Definition 10. Let δ_{g_0} is the Dirac delta measure supported on the point g_0 . We can define a measure on the limit set Λ by

$$\nu_\delta(A) = \lim_{t \searrow \delta} \frac{1}{t - \delta} \cdot \frac{\sum_{g \in \Gamma} \delta_{g_0}(A) e^{-td(0, g_0)}}{\sum_{g \in \Gamma} e^{-\delta d(0, g_0)}}, \quad A \subset \Lambda.$$

This is the standard construction of the Patterson–Sullivan measure on Λ (cf. a book of Nicholls [29, Ch. 3], for example). Although for each parameter t we obtain a measure on the countable set of points in the orbit of the point x_0 , and these measure live on the open disk and give zero measure to the boundary circle (and the limit set). As t decreases more weight is given to points closer to the boundary (in the Euclidean metric). In the limit these measures converge in the weak- $*$ topology of measures (on the closed unit disk) to a measure actually supported on the boundary circle.

We use the Patterson–Sullivan measure ν_δ and the Lebesgue measure along the flow direction dt to define a flow invariant measure $\widehat{\nu}_\delta$ on the unit tangent bundle to the universal cover, which can be identified with $(\partial\mathbb{D} \times \partial\mathbb{D} \setminus \text{diagonal}) \times \mathbb{R}$ by:

$$d\widehat{\nu}_\delta(x, y, t) = \frac{d\nu_\delta \times d\nu_\delta \times dt}{|x - y|^{2\delta}}$$

This corresponds to an invariant measure on $\partial\mathbb{D} \times \partial\mathbb{D}$ under the diagonal action of Γ , i.e., $g(x, y) = (gx, gy)$. Finally, by considering the quotient by Γ and normalizing we arrive at a φ_t -invariant measure ν on the unit tangent bundle Y .

Similarly to the compact case (Definition 6), given two smooth functions $F, G: Y \rightarrow \mathbb{R}$ we define the correlation function associated to the flow φ_t by

$$\rho(t) = \int_Y (F \circ \varphi_t) G d\nu - \int_Y F d\nu \int_Y G d\nu$$

In the case of infinite area surfaces the approach of unitary representations does not apply so naturally. However, there are dynamical approaches, mostly rooted in the work of Dolgopyat [12], that gives an analogue to Theorem 4.

Theorem 7 (Naud, 2005). *There exists $C, \varepsilon > 0$ such that $|\rho(t)| \leq Ce^{-\varepsilon t}$ for $t \geq 0$.*

The proof makes use of transfer operators. These are used to analyze the Laplace transform $\hat{\rho}$ by showing that the resolvent of the transfer operator \mathcal{L}_s given by (4) has no poles for $\Re(s) \geq -\varepsilon$.

8 Location of resonances for infinite area surfaces

Finally, we want to discuss the behaviour of the distribution of the zeros for the analytic extension of the Selberg zeta function in the case of infinite area surfaces.

8.1 Rigorous results: the case of pair of pants

To demonstrate the method, we will consider the case of a pair of pants. This is the simplest example to study and in this case the results are clearer to interpret. However, the analysis can be adapted to other examples and some of these are discussed in the last section.

8.1.1 Distribution of zeros

Since the Hausdorff dimension corresponds to the parameter value when the operator \mathcal{L}_s has maximal eigenvalue 1, and the zeta function is $\det(I - \mathcal{L}_s)$, we may deduce that $Z_V(\delta) = 0$. We also know [27] that there are no zeros in a (possibly very) small strip $\delta' < \Re(s) < \delta$. A natural question so ask is what happens when we first venture into the region $\Re(s) < \delta'$?

Question 7. What about the other zeros not so near $\Re(s) = \delta$?

Since we expect that there will be zeros in a larger region, it is therefore more appropriate to ask about the density of zeros. Naud showed the following:

Theorem 8 (Naud, 2014). *Fix $\sigma \in (\frac{\delta}{2}, \delta)$. Then there exists $0 < \eta < \delta$:*

$$\#\{s_n = \sigma_n + it_n \mid Z_V(s_n) = 0: \sigma \leq \sigma_n \leq \delta, |t_n| \leq t\} = O(t^{1+\eta}).$$

The proof is particularly elegant and uses both the Bowen–Series map and properties of the pressure.

8.1.2 Patterns of zeros

Our final result concerns the strange patterns of zeros that one sees empirically. Consider again the example of a pair of pants and associate the Selberg zeta function (cf. (5))

$$Z_V(s) = \prod_{n=0}^{\infty} \prod_{\gamma} (1 - e^{-(s+n)\ell(\gamma)}), \quad s \in \mathbb{C},$$

where γ is a (prime) closed geodesic or an orbit of the flow of length $\ell(\gamma)$. We have already mentioned (cf. Lemma 20) that the infinite product converges for $\Re(s) > \delta = \dim_H \Lambda$, the Hausdorff dimension of the limit set of the associated Bowen–Series map and there is an analytic extension to \mathbb{C} , that can be established using trace of the associated transfer operator.

The main object of study in this section is the zero set of the function Z_V :

$$\mathcal{S}_V := \{s \in \mathbb{C} \mid Z_V(s) = 0\}. \tag{6}$$

Question 8. Where are the zeros of $Z_V(s)$, in strip $0 < \Re(s) < \delta$ located?

In pioneering experimental work, D. Borthwick has studied the location of the zeros for the zeta function in specific examples of infinite area surfaces [5]. The plot in Figure 8 is fairly typical for zeros in the critical strip for a symmetric three funnelled surface where each of the three simple closed geodesics corresponding to a funnel has the same, sufficiently large, length. A modern laptop allows one to study symmetric three funnelled surface with the length of the three defining closed geodesics at least 8 without much difficulty.

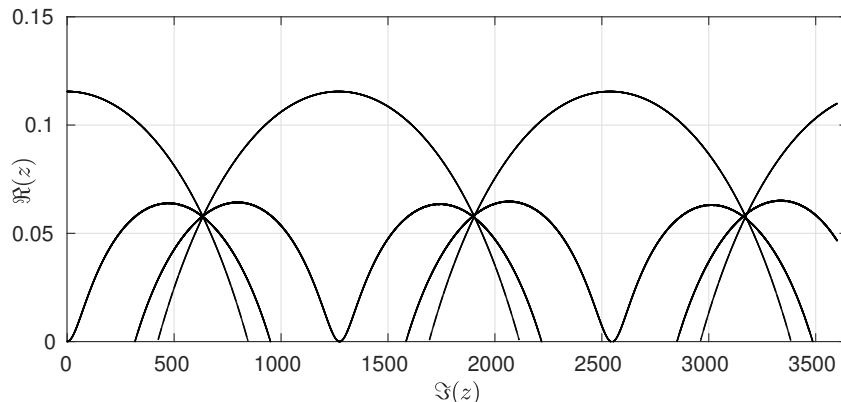


Figure 8: The zeros of the associated zeta function Z_V in the critical strip. The individual zeros are so close in the plot that it creates the illusion that they form well defined smooth curves.

Based on numerical evidence, we make the following simple empirical observations

Informal Qualitative Observations. Let $V = V(b)$ be the three funnelled surface defined by three simple closed geodesics of equal length⁵ $2b$ then for a sufficiently large b :

O1 : The set of zeros \mathcal{S}_V *appears* to be an almost periodic set with translations

$$\tau = \{i(\pi k e^b + \varepsilon_k) \mid k \in \mathbb{N}\}$$

where $\varepsilon_k = \varepsilon_k(b) = o(e^{-b/2})$ as $b \rightarrow +\infty$ for each k .

O2 : The set of zeros \mathcal{S}_V *appears* to lie on a few distinct curves, which *seem* to have a common intersection point at $\frac{\delta}{2} + i\frac{\pi}{2}e^b$, as $b \rightarrow +\infty$.

One way to understanding these observations is to find an approximation of the zeta function by a simpler expressions whose zero set can be described. The first obstacle is that for large b the value of $\delta = \dim_H \Lambda$ will be small. We begin by recalling the following result of McMullen [25]:

Lemma 21. *The largest real zero $\delta \sim \frac{\ln 2}{b}$ as $b \rightarrow +\infty$, i.e., $\lim_{b \rightarrow +\infty} b\delta = \ln 2$.*

⁵This normalization makes formulae in subsequent calculations shorter.

It gives us the width of the critical strip: we see immediately that in the limit $b \rightarrow +\infty$ the zero set “converges” to the imaginary axis. We therefore apply an affine rescaling that allows us to see the pattern in the zero set for large values of b . A natural choice for rescaling factors is the approximate period of the pattern in the imaginary direction and the approximate reciprocal of the width of the critical strip in the real direction.

Notation. *We will be using the following notation.*

(a) *A compact part of the critical strip of height $h > 0$ which we denote by*

$$\mathcal{R}(h) = \{s \in \mathbb{C} \mid 0 \leq \Re(s) \leq \delta \text{ and } |\Im(s)| \leq h\};$$

and a compact part of the normalized critical strip of height $\hat{h} > 0$ which we denote by

$$\widehat{\mathcal{R}}(\hat{h}) = \{s \in \mathbb{C} \mid 0 \leq \Re(s) \leq \ln 2 \text{ and } |\Im(s)| \leq \hat{h}\}.$$

(b) *We denote the rescaled set of zeros by*

$$\widehat{\mathcal{S}}_V := \left\{ \sigma b + ie^{-bt} \mid \sigma + it \in \mathcal{S}_V \right\}.$$

where evidently, $0 < \Re(\widehat{\mathcal{S}}_V) \leq \ln 2$.

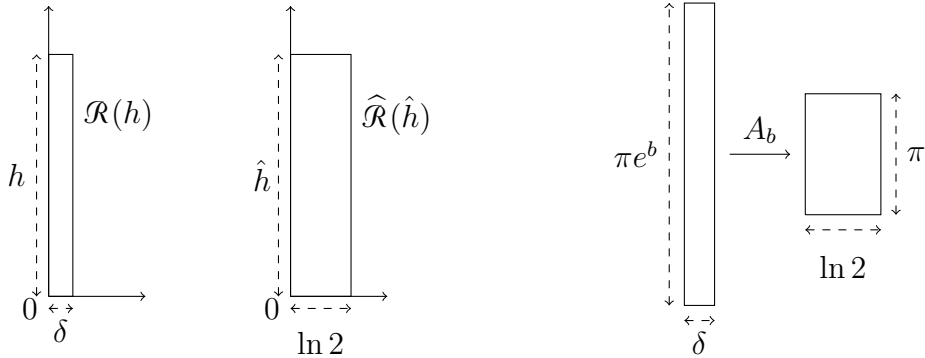


Figure 9: Left: The strips $\mathcal{R}(h)$ and $\widehat{\mathcal{R}}(\hat{h})$; Right: By renormalizing the strip $\mathcal{R}(\pi e^b)$ to $\widehat{\mathcal{R}}(\pi)$ we can compare the zeros of zeta functions for different b , as b tends to infinity.

We now introduce a family of four curves approximating $\widehat{\mathcal{S}}_V$ as $b \rightarrow +\infty$.

(c) *Let $\mathcal{C} = \cup_{j=1}^4 \mathcal{C}_j$, where the \mathcal{C}_i are explicit curves given by*

$$\begin{aligned} \mathcal{C}_1 &= \left\{ \frac{1}{2} \ln |2 - 2 \cos(t)| + it \mid \frac{\pi}{3} \leq t \leq \pi \right\}; \\ \mathcal{C}_2 &= \left\{ \frac{1}{2} \ln |2 + 2 \cos(t)| + it \mid 0 \leq t \leq \frac{2\pi}{3} \right\}; \\ \mathcal{C}_3 &= \left\{ \frac{1}{2} \ln \left| 1 - \frac{1}{2} e^{2it} - \frac{1}{2} e^{it} \sqrt{4 - 3e^{2it}} \right| + it \mid 0 \leq t \leq \frac{3\pi}{4} \right\}; \\ \mathcal{C}_4 &= \left\{ \frac{1}{2} \ln \left| 1 - \frac{1}{2} e^{2it} + \frac{1}{2} e^{it} \sqrt{4 - 3e^{2it}} \right| + it \mid \frac{\pi}{4} \leq t \leq \pi \right\}. \end{aligned}$$

The key thing to note is that the curve \mathcal{C} in Figure 10 look very similar to empirical plots in Figure 12.

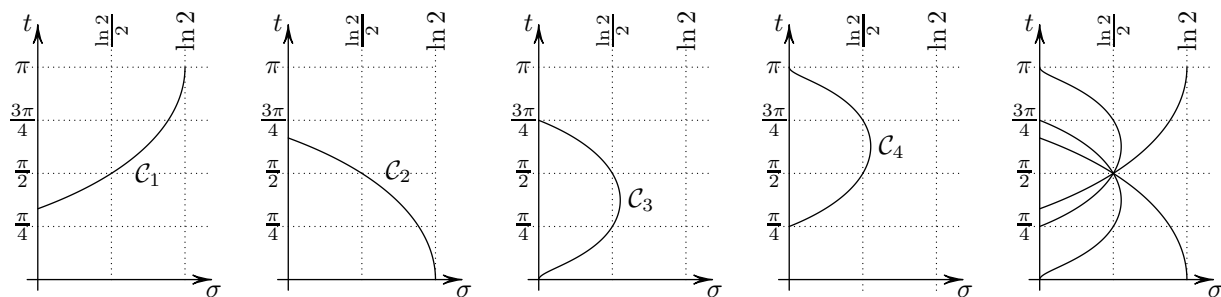


Figure 10: Plots of the curves \mathcal{C}_1 , \mathcal{C}_2 , \mathcal{C}_3 , \mathcal{C}_4 and their union \mathcal{C} .

We can now formally state the approximation result, which provides an explanation for the Observations.

Theorem 9. *The sets $\widehat{\mathcal{S}}_V$ and \mathcal{C} are close in the Hausdorff metric d_H on a large part of the strip $0 < \Re(s) < \log 2$. More precisely, there exists $\varkappa > 0$ such that*

$$d_H(\widehat{\mathcal{S}}_V \cap \widehat{\mathcal{R}}(e^{zb}), \mathcal{C} \cap \widehat{\mathcal{R}}(e^{zb})) \rightarrow 0 \text{ as } b \rightarrow +\infty.$$

The theorem implies that every rescaled zero $s \in \widehat{\mathcal{S}}_{V(b)} \cap \widehat{\mathcal{R}}(e^{zb})$ belongs to a neighbourhood of \mathcal{C} which is shrinking as $b \rightarrow \infty$. On the other hand, the rescaled zeros are so close, that the union of their shrinking neighbourhoods contains \mathcal{C} . The most significant feature of this result is that the height e^{zb} of the rescaled strip $\widehat{\mathcal{R}}(e^{zb})$ is larger than the period of the curves \mathcal{C} , and it corresponds to a part of the original strip of the height $e^{(1+\varkappa)b}$.

Because of the natural symmetries of $V(b)$, it is convenient to choose a presentation of the associated Fuchsian group in terms of three reflections (as in [25], for example). More precisely, we can fix a value $0 < \alpha \leq \frac{\pi}{3}$ and consider the Fuchsian group $\Gamma = \Gamma_\alpha := \langle R_1, R_2, R_3 \rangle$ generated by reflections R_1, R_2, R_3 in three disjoint equidistant geodesics $\beta_1, \beta_2, \beta_3$. In the previous description of the Bowen–Series coding we chose our generators to be orientation preserving. However, to exploit the symmetry of V these orientation reversing generators are more convenient, although the same general theory applies as before.

Although the three individual generators are orientation reversing the resulting quotient surface \mathbb{D}/Γ is an oriented infinite area surface. We now explain the pattern of the zeros for Z_V (for large b) in terms of those of a simpler approximating function.

8.1.3 Approximating Selberg zeta function

Finally, we come to a peculiar issue.

Question 9. Where do these curves come from?

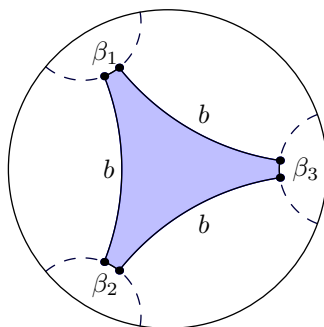


Figure 11: Three circles of reflection in Poincaré disk with pairwise distance b .

Consider the 6×6 complex matrix function

$$B(z) = \begin{pmatrix} 1 & z & 0 & 0 & z^2 & z \\ z & 1 & z^2 & z & 0 & 0 \\ 0 & 0 & 1 & z & z & z^2 \\ z^2 & z & z & 1 & 0 & 0 \\ 0 & 0 & z & z^2 & 1 & z \\ z & z^2 & 0 & 0 & z & 1 \end{pmatrix}$$

We can use this to give an approximation to Z_V and its zeros.

Theorem 10 (Approximation Theorem). *Using the notation introduced above, the real analytic function $Z_V(\frac{\sigma}{b} + ite^b)$ converges uniformly to $\det(I - \exp(-2\sigma - 2itbe^b)B(e^{it}))$, i.e.,*

$$\left| Z_V\left(\frac{\sigma}{b} + ite^b\right) - \det(I - \exp(-2\sigma - 2itbe^b)B(e^{it})) \right| \rightarrow 0 \text{ as } b \rightarrow +\infty.$$

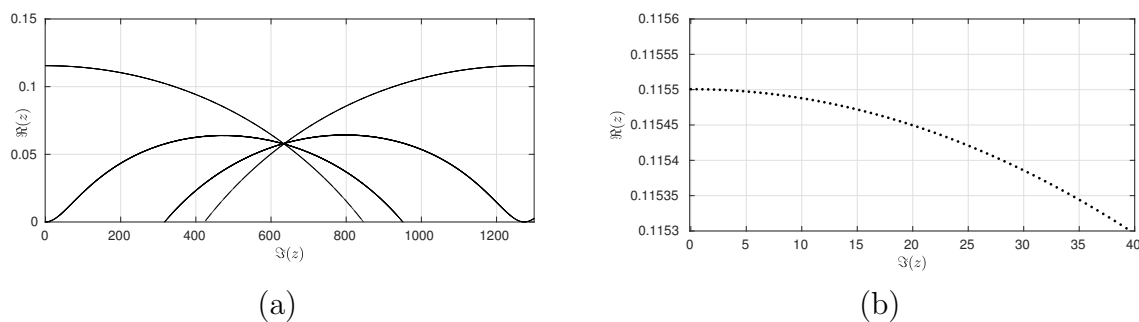


Figure 12: (a) The zeros of the determinant $\det(I - e^{-2b\sigma}B(\exp(ie^{-b}t)))$ approximating $Z_V(b)$; (b) A zoomed version in a neighbourhood of δ showing individual zeros. The distance between imaginary parts of consecutive zeros is approximately $\frac{\pi}{b}$.

Key observation: The importance of the matrix B is that for $s = \sigma + it$ to lie on the curves $\mathcal{C}_1, \mathcal{C}_2, \mathcal{C}_3, \mathcal{C}_4$ corresponds to eigenvalues λ_t for $B(e^{-it})$ to satisfy $e^{-\sigma}|\lambda_t| = 1$.

We will briefly explain how Theorem 10 implies Theorem 9. We shall show that for all $\varepsilon > 0$ and $T > 0$ there exists $b_0 > 0$ such that for any $b > b_0$ the zeros of the function $Z\left(\frac{\sigma}{b} + ite^b\right)$ with $0 \leq \sigma \leq \ln 2$ and $|t| \leq e^{(2-\varepsilon)b}$ belong to a neighbourhood $\cup_k U(\mathcal{C}_k, \varepsilon)$ of the union of the curves $\cup_k \mathcal{C}_k$.

Given $\varepsilon > 0$ and a point $z_0 = \sigma_0 + it_0$ outside of ε -neighbourhood of $\cup_{j=1}^4 \mathcal{C}_j$ a straightforward computation gives that the determinant

$$|\det(I - \exp(-2\sigma_0 - it_0 b e^b) B(\exp(it_0)))| > \exp(-6\varepsilon)(\exp \varepsilon - 1)^6 > 0$$

is bounded away from zero and the bound is independent of b . Thus we see that outside of the neighbourhood $\cup_{j=1}^4 U(\mathcal{C}_j, \varepsilon)$ the determinant has modulus uniformly bounded away from 0. But using Theorem 10 the zeta function $Z_V\left(\frac{\sigma}{b} + ite^b\right)$ can be approximated arbitrarily closely by the determinant. Therefore for b sufficiently large all zeros of the function $Z_V\left(\frac{\sigma}{b} + ite^b\right)$ belong to the ε -neighbourhood of $\cup_{j=1}^4 \mathcal{C}_j$.

8.2 The case of one-holed torus

In this section we want to apply ideas developed in [34] and described above to study patterns of zeros of the Selberg zeta function associated to a symmetric one-holed torus. Contrary to the case of a pair of pants, they still remain a mystery, and our goal here is to formulate a few conjectures on the distributions of zeros, and to give more insight into our approach. We try to make this section as self-contained as possible, though we reuse the notation.

The Selberg zeta function corresponding to the holed torus is the same as the one associated to a genus one hyperbolic surface with a single funnel, the case studied by D. Borthwick and T. Weich [5], [8]. We start with numerical experiments.

8.2.1 Plots of zeros and conjectures

It is well-known that, as a Riemann surface, a one-holed torus is uniquely defined by the length of two shortest geodesics and the angle in between as shown in Figure 13. We say that a one-holed torus is symmetric if the two geodesics have the same length and are orthogonal to each other. Therefore a symmetric one-holed torus has only one parameter and we will denote it by $\mathring{\mathbb{T}}(a)$, where a is the length of the shortest closed geodesic. We would like to consider three different symmetric tori⁶ $\mathring{\mathbb{T}}(10)$, $\mathring{\mathbb{T}}(14 \log 2 + 0.05)$, and $\mathring{\mathbb{T}}(14 \log 2)$.

It is known [25] that the width of the critical strip is proportional to a^{-1} . Physical dimensions of paper and screen impose limitations on the figures. To make them more realistic, we plot

⁶This choice will be clear later, here we just note that the first choice $a = 10$ is guided by previous research [5] and the integer part $\left\lfloor \frac{10}{\log 2} \right\rfloor = 14$.

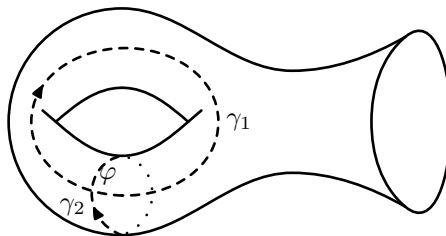


Figure 13: One-funneled torus with Fenchel–Nielsen coordinates: a pair of shortest geodesic γ_1 , γ_2 and angle inbetween φ . Artistic impression. There is no embedding into \mathbb{R}^3 .

rescaled zeros and chose aspect ratio of the image to correspond the scale on the axis. In addition, the algorithm we are using allows to compute the zeros in a small part of the critical strip near the real axis $0 < \Re z < \delta$, $0 < \Im z < e^{\frac{3a}{2}}$ only. We refer to this subset of the zero set as “small zeros”, and these are *the only zeros we consider here*, unless stated otherwise.

Three sample plots are shown in Figure 14. The plot in Figure 14(b) corresponds to a small region of the plot in [13], p. 30, Fig. 7 (bottom) near the imaginary axis, and the plot in Figure 14(c) corresponds to the plot in [5], p. 7, Fig. 11 (left).

We will be using the following notation. Let

$$\widehat{S}(a) = \widehat{S}_{\mathring{\mathbb{T}}(a)} \stackrel{\text{def}}{=} \left\{ \hat{z} = a (\Re z + e^{-2a} \Im z) \mid Z_{\mathring{\mathbb{T}}(a)}(z) = 0, 0 < \Im z < e^{\frac{3a}{2}} \right\} \quad (7)$$

be a set of small rescaled zeros of the zeta function $Z_{\mathring{\mathbb{T}}(a)}$ associated to the torus $\mathring{\mathbb{T}}(a)$.

Based on numerical experiments we state several conjectures on properties of small rescaled zeros, which we will try to explain heuristically in Section §8.2.4, leaving rigorous arguments for another occasion.

To characterise the density of the set of small zeros we define a cover by open balls of a given set A by

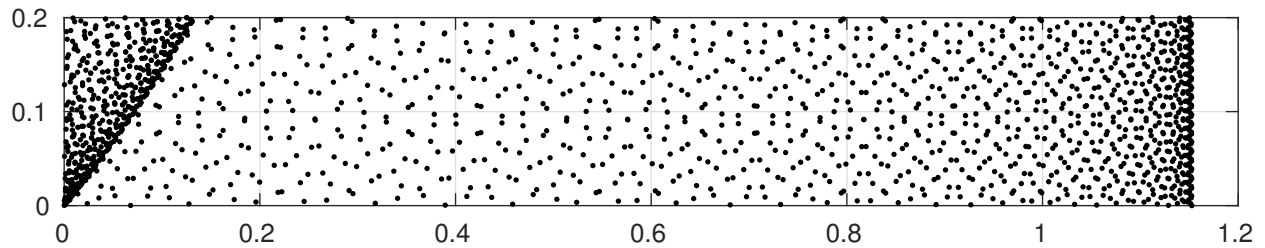
$$Cr(A) = \bigcup_{z \in A} B(z, r(z)), \text{ where } r(z) = \min_{z' \neq z, z' \in A} |z - z'|. \quad (8)$$

The plots illustrating the cover in the cases which we consider are shown in Figure 15.

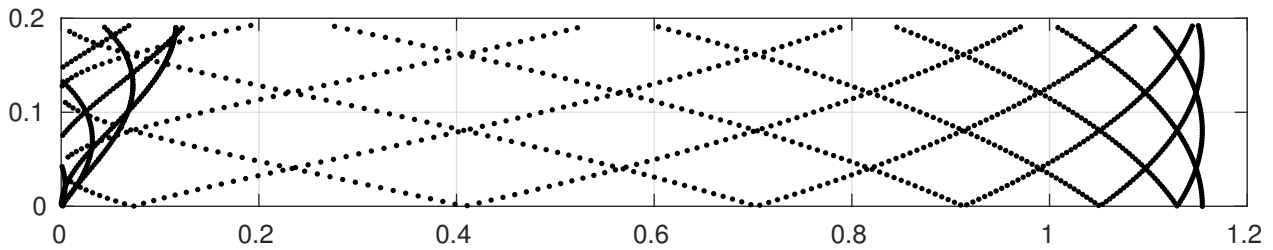
In order to describe differences between the sets of small rescaled zeros corresponding to different tori, we will study the dependence of the following characteristics on the length parameter a .

1. The Hausdorff distance between the convex hull of the set of small rescaled zeros and the set itself $D_H(a) \stackrel{\text{def}}{=} \text{dist}_H(\text{Conv}(\widehat{S}(a)), \widehat{S}(a))$;
2. The area of the cover $M(a) \stackrel{\text{def}}{=} \text{Area}(Cr(\widehat{S}(a)))$;
3. Expectation $E(a) \stackrel{\text{def}}{=} \mathbb{E}(\inf |z - \widehat{S}(a)|)$ and variance $V(a) = \text{Var}(\inf |z - \widehat{S}(a)|)$ of the distance from a randomly chosen point z in the critical strip to $\widehat{S}(a)$.

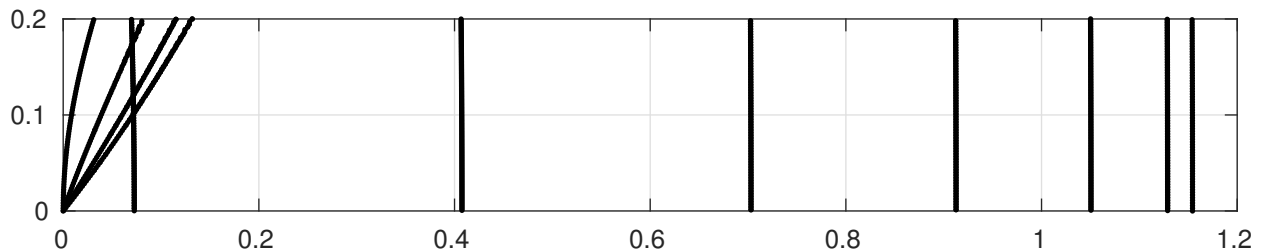
Figure 14: Characteristic plots of rescaled zeros of symmetric torus. Larger balls mean that the rescaled zeros are further away. In all three subfigures $a \cdot e^{-\frac{a}{2}} \approx 0.07$ and we show the strip $0 < \Im \hat{z} < 0.2 \approx 3 \cdot 0.07$.



(a) The plot shows 1777 rescaled zeros $\hat{z} \in \widehat{S}(10)$, $0 < \Im \hat{z} < 0.2$.



(b) The plot shows 1382 rescaled zeros $\hat{z} \in \widehat{S}(14 \log 2 + 0.05)$, $0 < \Im \hat{z} < 0.2$.



(c) The plot shows 1359 rescaled zeros $\hat{z} \in \widehat{S}(14 \log 2)$, $0 < \Im \hat{z} < 0.2$.

Table 2: Hausdorff distance, expectation, variance, and area of the cover.

a	$\left\{\frac{a}{\log 2}\right\}$	$D_H(a)$	$M(a)$	$E(a)$	$V(a)$
$14 \log 2$	0	0.1671...	0.130210...	0.040...	0.001...
$14 \log 2 + 0.05$	0.072...	0.0356...	0.901338...	0.010...	$5.1 \dots \cdot 10^{-5}$
10	0.427...	0.0041...	1.060217...	0.006...	$9.6 \dots \cdot 10^{-6}$

A selection of three representative empirical results is shown in Table 2. On the basis of these (over 100 many) results we propose the following conjecture.

Conjecture 1 (distribution of rescaled zeros near the real axis). *The Hausdorff distance D_H , the area function M , the expectation E , and the variance V are continuous and monotone functions with respect to the fractional part $\left\{\frac{a}{\log 2}\right\}$. In particular, D_H and M are increasing while E and V are decreasing. Therefore, $a \in \mathbb{N} \log 2$ are local maxima for E and V , and local minima for D_H and M .*

In the case of $\mathring{\mathbb{T}}(k \log 2)$ for some $k \in \mathbb{N}$ small zeros can be described more precisely.

Conjecture 2 (the case of rationally-dependent short geodesics). *Let $a \in \mathbb{N} \log 2$. Small zeros with $0 < \Im z \leq e^{\frac{3a}{2}}$ lie on a small number of well defined lines. Among them, there are $\frac{a}{\log 2}$ lines nearly parallel to the imaginary axis if $\frac{a}{\log 2}$ is odd, and $\frac{a}{2 \log 2}$ lines nearly parallel to the imaginary axis if $\frac{a}{\log 2}$ is even.*

The following conjecture addresses properties of the non-rescaled zero set of $Z_{\mathring{\mathbb{T}}(a)}^*$ independently of number-theoretic properties of a .

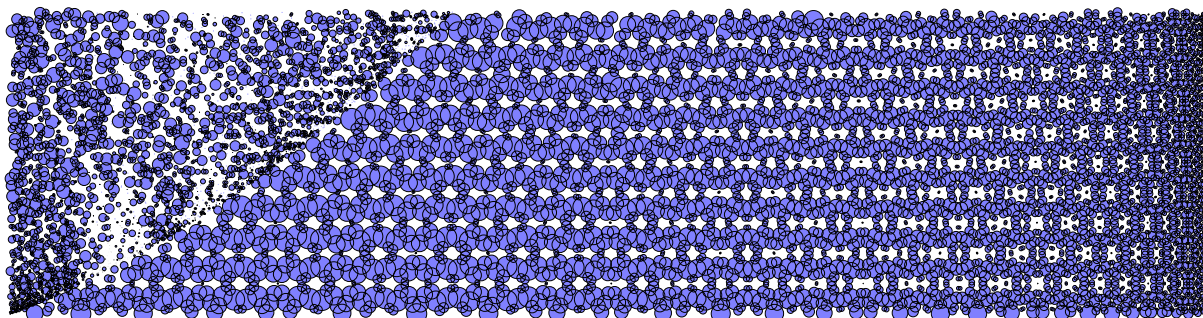
Conjecture 3 (distribution of zeros on a large scale). *The zero set of the Selberg zeta function for $\mathring{\mathbb{T}}(a)$ has the following properties*

1. *The asymptotic of the number of zeros in the critical strip with $\Im z < t$ is*

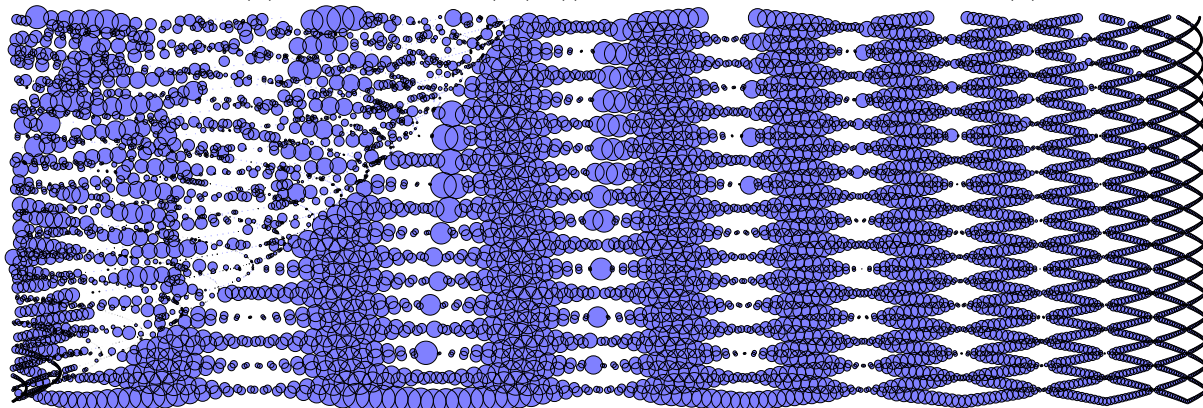
$$\#\{z \in \mathbb{C} \mid 0 < \Re z < \delta, 0 < \Im z < t, Z_{\mathring{\mathbb{T}}(a)}(z) = 0\} = \frac{2a}{\pi}t + O(1);$$

2. *Any rectangle in the critical strip of the height $\frac{\pi}{a}$ contains at least one zero;*
3. *The real parts of zeros are dense in $(0, \frac{1}{2}\delta)$.*

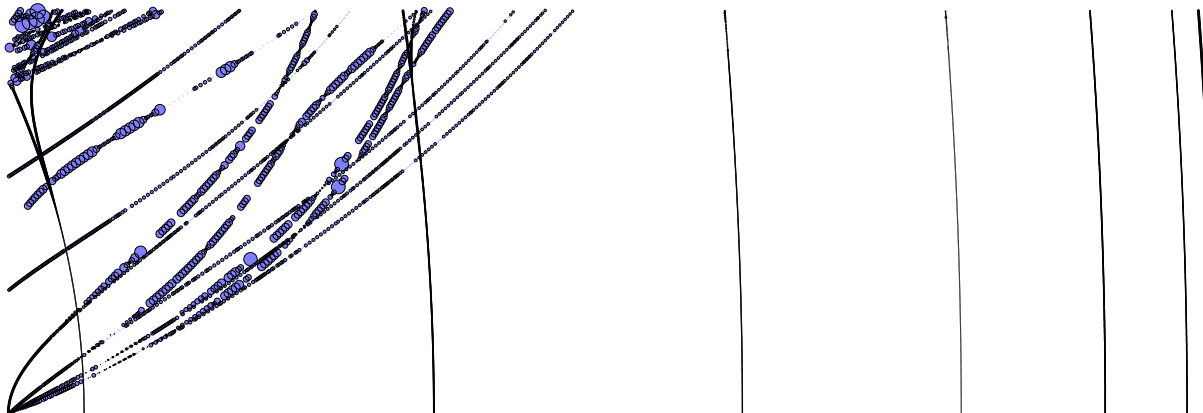
Figure 15: Characteristic plots of rescaled zeros with a cover by disks of the radius equal to the distance to the nearest zero. Bigger disks mean that the zeros are further apart.



(a) The cover $Cr(\widehat{S}(10))$ of the zero set from Figure 14(a).



(b) The cover $Cr(\widehat{S}(14 \log 2 + 0.05))$ of the zero set from Figure 14(b).



(c) The cover $Cr(\widehat{S}(14 \log 2))$ of the zero set from Figure 14(c).

Table 3: Dispersion and expectation of the distance to the zero set measured using different choices of sample points.

Sample point distribution	Expectation	Dispersion
Symmetric torus $a = 14 \log 2$		
regular rectangular 100×50000 points	0.040454...	0.001345...
random 50×1000 points	0.040417...	0.001347...
random 100×50000 points	0.040361...	0.001347...
Symmetric torus $a = 14 \log 2 + 0.05$		
regular rectangular 100×50000 points	0.010254...	$5.135236 \dots \cdot 10^{-5}$
random 50×1000 points	0.010212...	$5.163147 \dots \cdot 10^{-5}$
random 100×50000 points	0.010218...	$5.148808 \dots \cdot 10^{-5}$
Symmetric torus $a = 10 = 14 \log 2 + 0.29 \dots$		
regular rectangular 100×50000 points	0.005994...	$9.705229 \dots \cdot 10^{-6}$
random 50×1000 points	0.006002...	$9.641849 \dots \cdot 10^{-6}$
random 100×50000 points	0.005972...	$9.657625 \dots \cdot 10^{-6}$

8.2.2 Geometry of a one-holed torus

A very good exposition can be found in Buser and Semmler [10]. Here we summarise the results we need making necessary adaptations to the case we consider. A one holed torus is a genus one Riemann surface whose boundary consists of a single simple closed geodesic. In order to estimate the length of the closed geodesics we use Fenchel—Nielsen coordinates and a universal cover by a holed plane. It turns out that in the case of symmetric one-holed torus the universal cover has one parameter. Namely, we may consider a right-angled hyperbolic pentagon with the sides $\{a, *, b, *, a\}$ as shown by the shaded area in Figure 16(a). It is known cf. [3], §7.18 that a and b satisfy the identity

$$\sinh^2 a = \cosh b.$$

Fixing the length of the boundary geodesic b we compute

$$a = \frac{1}{2} \ln \left(e^b + e^{-b} + 1 + \sqrt{e^{2b} + e^{-2b} + 2(e^b + e^{-b}) + 1} \right) = \frac{1}{2} \left(b + \log 2 + e^{-b} + \frac{1}{3} e^{-3b} + o(e^{-3b}) \right). \quad (9)$$

We can glue together four identical pentagons Q and obtain a hyperbolic right-angled octagon \tilde{Q} as shown in Figure 16(a). The octagon is uniquely determined up to an isometry by b , which can vary freely in $(0, +\infty)$.

For visualisation purposes, consider the octagon \tilde{Q} as an ordinary right-angled octagon on \mathbb{R}^2 plane, with four quarters of a circle as alternating sides and other four sides parallel to coordinate axis. We assign labels ∇ and Δ to two sides parallel to the horizontal axis and

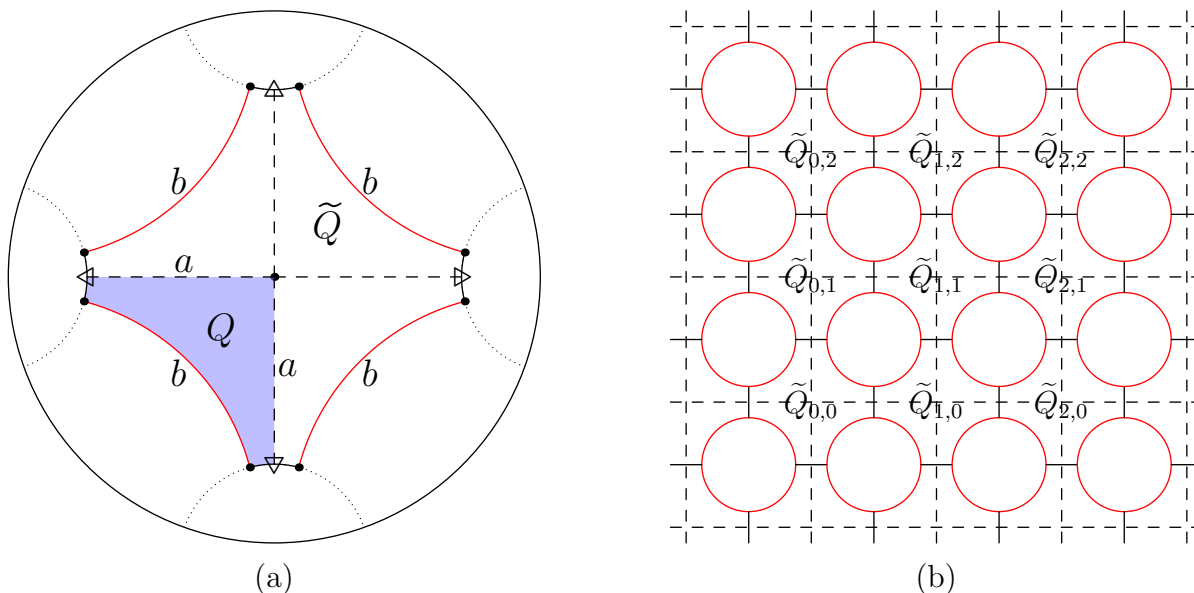


Figure 16: (a) A right-angled hyperbolic pentagon Q and its three copies forming a fundamental domain \tilde{Q} in the Poincaré disk. (b) A tessellation of $\mathbb{Z} \times \mathbb{Z}$ -holed real plane by copies of the fundamental domain $\tilde{Q}_{i,j}$.

\triangleright and \triangleleft to the sides parallel to the vertical axis. Translating the octagon along vertical and horizontal axes we obtain a tessellation of a holed plane Ω , where the holes are Euclidean disks made of four quarters of the boundary circles glued together, as shown in Figure 16(b). The holed plane Ω is a universal cover of a symmetric one-holed torus, and carries the hyperbolic structure of \tilde{Q} . Evidently there is a natural action of the group $\Gamma = \mathbb{Z} \times \mathbb{Z}$ on Ω by isometries and copies $\tilde{Q}_{i,j}$ of \tilde{Q} are fundamental domains. Two dashed lines in \tilde{Q} give a pair of shortest closed geodesics in Ω/Γ , which are generators of the fundamental group.

We can use the local isometry between the plane and the torus with hyperbolic metric in order to estimate the lengths of closed geodesics.

It is known that every closed oriented geodesic γ on Ω/Γ is freely homotopic to a periodic word $\dots \triangle^{n_1} \triangleright^{k_1} \triangle^{n_2} \triangleright^{k_2} \dots \triangle^{n_t} \triangleright^{k_t} \dots$ of period $\omega(\gamma) \stackrel{\text{def}}{=} |n_1| + \dots + |n_t| + |k_1| + \dots + |k_t|$ where n_j and k_j are integers and $\triangleleft = \triangleright^{-1}$, $\triangle = \nabla^{-1}$. We denote this geodesic by

$$\gamma_{(\triangle^{n_1} \triangleright^{k_1} \triangle^{n_2} \triangleright^{k_2} \dots \triangle^{n_t} \triangleright^{k_t})},$$

and we call the periodic sequence $(\triangle^{n_1} \triangleright^{k_1} \triangle^{n_2} \triangleright^{k_2} \dots \triangle^{n_t} \triangleright^{k_t})$ the cutting sequence associated to the closed geodesics. A good exposition on cutting sequences associated to closed geodesics on a one-holed torus can be found in [39].

The homotopy is unique up to conjugation by fundamental group. In particular, the two shortest geodesics correspond to the “constant” sequences of period one (\triangleright) and (∇).

The homotopy defines a bijection between closed geodesics and periodic two-sided infinite sequences $\{\sigma_k\}_{-\infty}^{\infty}$ in the alphabet $\Sigma = \{\triangle, \nabla, \triangleright, \triangleleft\}$ which satisfy an additional condition

that $\sigma_k \neq \sigma_{k+1}^{-1}$ for any $k \in \mathbb{Z}$. We define a transition matrix

$$\mathbb{A} = \begin{pmatrix} 1 & 0 & 1 & 1 \\ 0 & 1 & 1 & 1 \\ 1 & 1 & 1 & 0 \\ 1 & 1 & 0 & 1 \end{pmatrix}.$$

Let $\Sigma^{\mathbb{A}}$ be the set of words which are freely homotopic to geodesics on Ω/Γ , and periodic words in $\Sigma^{\mathbb{A}}$ correspond to closed geodesics. The shift on $\Sigma^{\mathbb{A}}$ corresponds to the action of Γ on closed geodesics.

It is easier to do the calculations using the upper half model $H = \{z \in \mathbb{C} \mid \Im z > 0\}$ of the hyperbolic plane and a subgroup of $PSL(2, \mathbb{R})$ acting on H . Namely, consider matrices

$$B = \begin{pmatrix} \cosh(a) & -\sinh(a) \\ -\sinh(a) & \cosh(a) \end{pmatrix} \quad C = \begin{pmatrix} e^a & 0 \\ 0 & e^{-a} \end{pmatrix}$$

Then the subgroup $\langle B, C \rangle \subset PSL(2, \mathbb{R})$ is a deck group of the universal cover $H \rightarrow \Omega/\Gamma$ and generators B and C correspond to the generators $\gamma_{(\nabla)}$ and $\gamma_{(\triangleright)}$ of the fundamental group of Ω/Γ . Moreover, the hyperbolic length of the geodesic corresponding to the cutting sequence $\dots \Delta^{n_1} \triangleright^{k_1} \Delta^{n_2} \triangleright^{k_2} \dots \Delta^{n_t} \triangleright^{k_t} \dots$ of period $\omega(\gamma) \stackrel{\text{def}}{=} |n_1| + \dots + |n_t| + |k_1| + \dots + |k_t|$, (where $k_j \neq 0$, $n_j \neq 0$ for $j = 1, \dots, t$) is given by

$$\ell(\gamma_{(\Delta^{n_1} \triangleright^{k_1} \Delta^{n_2} \triangleright^{k_2} \dots \Delta^{n_t} \triangleright^{k_t})}) = 2 \operatorname{ArcCosh} \left(\frac{1}{2} \left| \operatorname{tr} (B^{n_1} C^{k_1} B^{n_2} C^{k_2} \dots B^{n_t} C^{k_t}) \right| \right). \quad (10)$$

8.2.3 Approximating determinant

Notation. Given a contiguous subsequence $\sigma_1, \dots, \sigma_k$ of a sequence $\sigma \in \Sigma^{\mathbb{A}}$ we denote by $\gamma_{\sigma_1, \dots, \sigma_k}$ a geodesic whose cutting sequence contains the contiguous subsequence $\sigma_1, \dots, \sigma_k$. We denote by $\gamma_{[\sigma_1, \dots, \sigma_k]}$ a segment of a geodesic whose cutting sequence contains a contiguous subsequence $\sigma_1, \dots, \sigma_k$ with end points at the midpoints of the segments enclosed between intersections with the sides σ_1, σ_2 and σ_{k-1}, σ_k . We denote by $\gamma_{[\sigma_1, \dots, \sigma_k]}$ the segment of the shortest of all closed geodesics whose cutting sequence contains the contiguous subsequence $\sigma_1, \dots, \sigma_k$ with end points at the midpoints of segments enclosed between intersections with the sides labelled σ_1, σ_2 and σ_{k-1}, σ_k , respectively (see Figure 17).

Let $\sigma^1, \dots, \sigma^N$ be all contiguous subsequences of sequences $\sigma \in \Sigma^{\mathbb{A}}$ of length n . Let us consider an $N \times N$ transition matrix given by

$$\mathbb{A}_{i,j}^n = \begin{cases} 1, & \text{if } \sigma_{k+1}^i = \sigma_k^j; \text{ for all } k = 1, 2, \dots, n-1. \\ 0, & \text{otherwise.} \end{cases}$$

We now define a one-parameter family of $N \times N$ matrices $A(s)$ which elements depend on the length of geodesic segments determined by σ^i and σ^j :

$$A: \mathbb{C} \rightarrow \operatorname{Mat}(N \times N) \quad A_{i,j}(s) = \mathbb{A}_{i,j}^n \cdot \exp(-s \cdot \ell(\gamma_{[\sigma_1^i \sigma_2^i \dots \sigma_n^i \sigma_n^j]})). \quad (11)$$

Note that A depends on n , but we omit this in the notation. We will be using the following Lemma from [34] to find the approximate location of the zeros.

Lemma 22. *Using the notation introduced above, we have the following representation for the Selberg zeta function*

$$Z_{\mathbb{H}(a)}(s) = \prod_{n=0}^{\infty} \prod_{\substack{\gamma=\text{primitive} \\ \text{closed geodesic}}} (1 - e^{-(s+n)\ell(\gamma)}) = \lim_{n \rightarrow \infty} \det(Id_n - A(s)), \quad (12)$$

where $Id_n \in \text{Mat}(n, n)$ is the identity matrix.

Our first Lemma gives approximations to lengths of geodesic segments.

Lemma 23.

$$\ell(\underline{\gamma}_{[\nabla\nabla\nabla]}) = 2a - \log \sqrt{2} + o(e^{-3a}) \quad \text{see Figure 18(a);} \quad (13)$$

$$\ell(\underline{\gamma}_{[\Delta\nabla\Delta]}) = 2a - \log 2 + 2e^{-2a} + o(e^{-3a}) \quad \text{see Figure 18(b);} \quad (14)$$

$$\ell(\underline{\gamma}_{[\Delta\nabla\nabla]}) = 2a - \log 2 - 2e^{-2a} + o(e^{-3a}) \quad \text{see Figure 17(b).} \quad (15)$$

Proof. The result follows by straightforward calculation by applying formula (10) together with (9) to $\gamma_{(\Delta\nabla\nabla\Delta)}$, $\gamma_{(\nabla\nabla\nabla\Delta)}$, and $\gamma_{(\Delta\nabla\Delta\Delta)}$, respectively. More precisely, by definition we have that

$$\begin{aligned} \ell(\underline{\gamma}_{[\Delta\nabla\nabla]}) &= \frac{1}{4} \ell(\gamma_{(\Delta\nabla\nabla\Delta)}) = \frac{1}{2} \text{ArcCosh} \left(\frac{1}{2} |\text{tr}(B^{-1}CBC^{-1})| \right) = \\ &= \frac{1}{2} \text{ArcCosh} \left(-\frac{e^{4a} + e^{-4a}}{8} + \frac{e^{2a} + e^{-2a}}{2} + \frac{1}{4} \right) = 2a - \log 2 - 2e^{-2a} - 5e^{-4a} + o(e^{-4a}). \end{aligned} \quad (16)$$

Similarly,

$$\begin{aligned} \ell(\underline{\gamma}_{[\nabla\nabla\nabla]}) &= \frac{1}{4} \ell(\gamma_{(\nabla\nabla\nabla\Delta)}) = \frac{1}{2} \text{ArcCosh} \left(\frac{1}{2} |\text{tr}(BBCC)| \right) = \\ &= \frac{1}{2} \text{ArcCosh} (\cosh^2 2a) = 2a - \log \sqrt{2} + 3e^{-4a} + o(e^{-6a}); \end{aligned} \quad (17)$$

And in the last case

$$\begin{aligned} \ell(\underline{\gamma}_{[\Delta\nabla\Delta]}) &= \frac{1}{4} \ell(\gamma_{(\Delta\nabla\Delta\Delta)}) = \frac{1}{2} \text{ArcCosh} \left(\frac{1}{2} |\text{tr}(B^{-1}CB^{-1}C)| \right) = \\ &= \frac{1}{2} \text{ArcCosh} \left(\frac{e^{4a} + e^{-4a}}{8} + \frac{e^{2a} + e^{-2a}}{2} - \frac{1}{4} \right) = 2a - \log 2 + 2e^{-2a} - 5e^{-4a} + o(e^{-4a}). \end{aligned} \quad (18)$$

■

In particular, we have the following corollary.

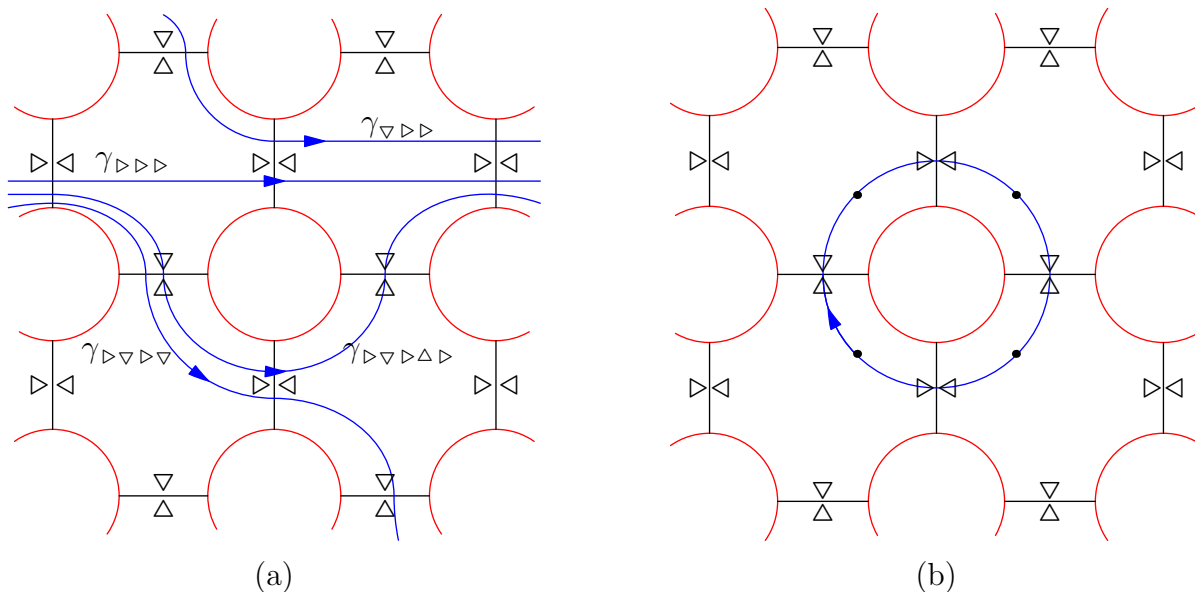


Figure 17: (a) Segments of geodesics lifted to the $\mathbb{Z} \times \mathbb{Z}$ holed plane, marked by contiguous subsequences of their cutting sequences, according to visible intersections. (b) The shortest closed geodesic among $\gamma_{\Delta\triangleright\triangleright}$ corresponding to periodic sequence $(\Delta\triangleright\triangleright\triangleleft)$ of period 4. The four marked points divide the geodesic into 4 equal segments: $\underline{\gamma_{[\Delta\triangleright\triangleright]}}$, $\underline{\gamma_{[\triangleright\triangleright\triangleleft]}}$, $\underline{\gamma_{[\triangleright\triangleleft\Delta]}}$, and $\underline{\gamma_{[\triangleleft\Delta\triangleright]}}$.

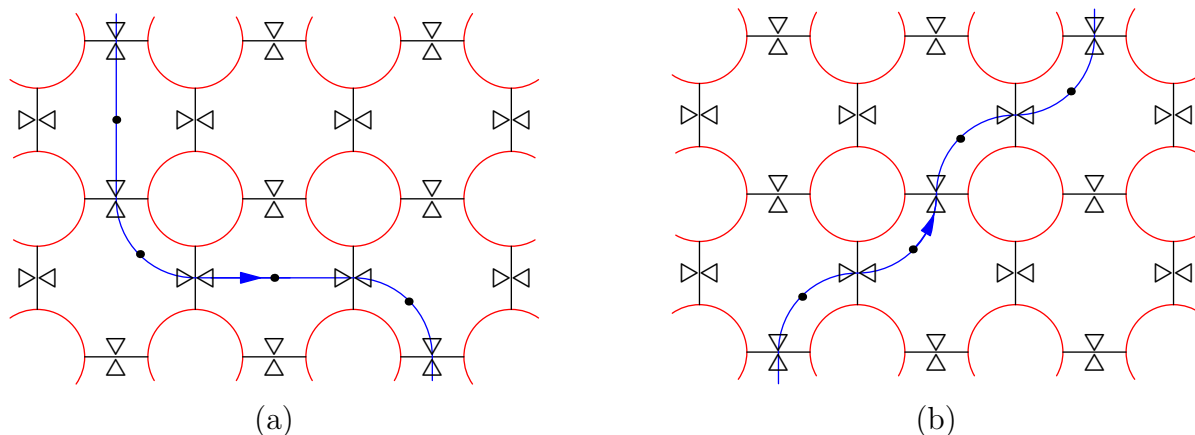


Figure 18: (a) The shortest closed geodesic among $\gamma_{\nabla\nabla\triangleright\triangleright}$, corresponding to the periodic sequence $(\nabla\nabla\triangleright\triangleright)$ of period 4. The four marked points divide the geodesic into 4 equal segments: $\underline{\gamma_{[\nabla\nabla\triangleright]}}$, $\underline{\gamma_{[\nabla\triangleright\triangleright]}}$, $\underline{\gamma_{[\triangleright\triangleright\triangleright]}}$, and $\underline{\gamma_{[\triangleright\nabla\nabla\triangleright]}}$. (b) The shortest closed geodesic among $\gamma_{\Delta\triangleright\triangleright\Delta}$, corresponding to the periodic sequence $(\Delta\triangleright\triangleright\Delta)$ of period 4. The four marked points divide the geodesic into 4 equal segments: $\underline{\gamma_{[\Delta\triangleright\triangleright]}}$, $\underline{\gamma_{[\triangleright\triangleright\Delta]}}$, $\underline{\gamma_{[\Delta\triangleright\Delta]}}$, and $\underline{\gamma_{[\triangleright\Delta\triangleright]}}$.

Corollary 2.

$$\ell(\underline{\gamma}_{[\sigma_1\sigma_2\sigma_3]}) = \begin{cases} 2a, & \text{if } \sigma_1 = \sigma_2 = \sigma_3; \\ 2a - \log \sqrt{2} + o(e^{-3a}), & \text{if } \sigma_1 = \sigma_2 \neq \sigma_3; \\ 2a - \log 2 - 2e^{-2a} + o(e^{-3a}), & \text{if } \sigma_1 = \sigma_3 \neq \sigma_2; \\ 2a - \log 2 + 2e^{-2a} + o(e^{-3a}), & \text{otherwise.} \end{cases}$$

Remark 5. This explains why the case $a = k \log 2$ is different. In particular, we see that this choice makes the length of short geodesics rationally dependent.

We now apply Corollary 2 to compute the matrix $A(s)$ for $n = 2$. There are 12 subsequences of length 2 of the sequences from $\Sigma^{\mathbb{A}}$. We can enumerate them as follows $\sigma^1 = \Delta\Delta$, $\sigma^2 = \Delta\triangleright$, $\sigma^3 = \Delta\triangleleft$, $\sigma^4 = \triangleright\triangleright$, $\sigma^5 = \triangleright\Delta$, $\sigma^6 = \triangleright\nabla$, $\sigma^7 = \nabla\nabla$, $\sigma^8 = \nabla\triangleright$, $\sigma^9 = \nabla\triangleleft$, $\sigma^{10} = \triangleleft\triangleleft$, $\sigma^{11} = \triangleleft\Delta$, $\sigma^{12} = \triangleleft\nabla$. Then using definition (11) we may compute, for example

$$A_{1,1}(s) = \exp(-s \cdot \ell(\underline{\gamma}_{[\Delta\Delta\Delta]})) = \exp(-2as);$$

$$A_{2,4}(s) = \exp(-s \cdot \ell(\underline{\gamma}_{[\Delta\triangleright\triangleright]})) = \exp(-2as) \cdot \sqrt{2^s} \cdot \exp(-s \cdot o(e^{-3a}));$$

$$A_{2,5}(s) = \exp(-s \cdot \ell(\underline{\gamma}_{[\Delta\triangleright\Delta]})) = \exp(-2as) \cdot 2^s \cdot \exp(2e^{-2a}s) \cdot \exp(-s \cdot o(e^{-3a}));$$

$$A_{2,6}(s) = \exp(-s \cdot \ell(\underline{\gamma}_{[\Delta\triangleright\nabla]})) = \exp(-2as) \cdot 2^s \cdot \exp(-2e^{-2a}s) \cdot \exp(-s \cdot o(e^{-3a}));$$

the other elements are similar. Observe that for values of s within the critical strip, $0 < \Re s < 0.2$, we have that $|\exp(-s \cdot o(e^{-3a})) - 1| \leq 2e^{-3a}$ is small for a sufficiently large. Introducing a short-hand notation

$$p_1(s) = \sqrt{2^s}; \quad (19)$$

$$p_2(a, s) = 2^{s+1} \cosh(2se^{-2a}); \quad (20)$$

$$p_3(a, s) = 2^{s+1} \sinh(2se^{-2a}); \quad (21)$$

we may consider a matrix

$$P(s) = \begin{pmatrix} 1 & p_1 & p_1 & 0 & 0 & 0 & 0 & 0 & 0 & 0 & 0 & 0 \\ 0 & 0 & 0 & p_1 & \frac{p_2-p_3}{2} & \frac{p_2+p_3}{2} & 0 & 0 & 0 & 0 & 0 & 0 \\ 0 & 0 & 0 & 0 & 0 & 0 & 0 & 0 & 0 & p_1 & \frac{p_2-p_3}{2} & \frac{p_2+p_3}{2} \\ 0 & 0 & 0 & 1 & p_1 & p_1 & 0 & 0 & 0 & 0 & 0 & 0 \\ p_1 & \frac{p_2-p_3}{2} & \frac{p_2+p_3}{2} & 0 & 0 & 0 & 0 & 0 & 0 & 0 & 0 & 0 \\ 0 & 0 & 0 & 0 & 0 & 0 & p_1 & \frac{p_2-p_3}{2} & \frac{p_2+p_3}{2} & 0 & 0 & 0 \\ 0 & 0 & 0 & 0 & 0 & 0 & 1 & p_1 & p_1 & 0 & 0 & 0 \\ 0 & 0 & 0 & p_1 & \frac{p_2+p_3}{2} & \frac{p_2-p_3}{2} & 0 & 0 & 0 & 0 & 0 & 0 \\ 0 & 0 & 0 & 0 & 0 & 0 & 0 & 0 & 0 & p_1 & \frac{p_2+p_3}{2} & \frac{p_2-p_3}{2} \\ 0 & 0 & 0 & 0 & 0 & 0 & 0 & 0 & 0 & 1 & p_1 & p_1 \\ p_1 & \frac{p_2+p_3}{2} & \frac{p_2-p_3}{2} & 0 & 0 & 0 & 0 & 0 & 0 & 0 & 0 & 0 \\ 0 & 0 & 0 & 0 & 0 & 0 & p_1 & \frac{p_2+p_3}{2} & \frac{p_2-p_3}{2} & 0 & 0 & 0 \end{pmatrix}.$$

Then the matrix $A(s)$ can be considered as a small perturbation of $\exp(-2as)P(s)$. By Lemma 2.8 from [34], the determinant $\det(I - A(s))$ approximates the Selberg zeta function. Since the matrices $\exp(-2as)P(s)$ and $A(s)$ are close, the determinant $\det(I - \exp(-2as)P(s))$ is an approximation to the zeta function, too. We see that the function $\det(I - \exp(-2as)P(s))$ is an exponential sum in s , and therefore an almost periodic function with modul $\langle a, \log 2, 2e^{-2a} \rangle$ if $a \notin \log 2\mathbb{Z}$ and $\langle \log 2, 4^{-k} \rangle$ otherwise. It follows from general theory of almost periodic functions that its zeros form a point-periodic set in the sense of Krein–Levin. The simplicity of the matrix P allows us to get more information on exact location of the zeros of the determinant. Evidently, the matrix $\exp(-2as)P(s)$ has an eigenvalue 1 if and only if $\exp(2as)$ is an eigenvalue of $P(s)$. The eigenvalues of the matrix $P(s)$ have a closed form.

$$\lambda_{1,2} = \pm p_3 \tag{22}$$

$$\lambda_{3,4} = \frac{1}{2} \left(1 - p_2 \pm \sqrt{(p_2 + 1)^2 - 8p_1^2} \right) \tag{23}$$

$$\lambda_{5,6} = \frac{1}{2} \left(1 + p_2 \pm \sqrt{(p_2 - 1)^2 + 8p_1^2} \right). \tag{24}$$

Introducing a shorthand notation $\tilde{p}(p_1, p_2, p_3) = 9p_3 \cdot (3p_1^2 - p_2) - 1$ we write the remaining eigenvalues, each of multiplicity 2, as follows:

$$\lambda_{7,8} = \frac{1}{3} \left(1 + \frac{3p_3p_2 - 1}{\sqrt[3]{\sqrt{\tilde{p}^2 - (3p_3p_2 - 1)^3} - \tilde{p}}} + \sqrt[3]{\sqrt{\tilde{p}^2 - (3p_3p_2 - 1)^3} - \tilde{p}} \right); \tag{25}$$

$$\lambda_{9,10} = \frac{1}{3} - \frac{i\sqrt{3} + 1}{6} \cdot \frac{3p_3p_2 - 1}{\sqrt[3]{\sqrt{\tilde{p}^2 - (3p_3p_2 - 1)^3} - \tilde{p}}} + \frac{i\sqrt{3} - 1}{6} \cdot \sqrt[3]{\sqrt{\tilde{p}^2 - (3p_3p_2 - 1)^3} - \tilde{p}}; \tag{26}$$

$$\lambda_{11,12} = \frac{1}{3} + \frac{i\sqrt{3} - 1}{6} \cdot \frac{3p_3p_2 - 1}{\sqrt[3]{\sqrt{\tilde{p}^2 - (3p_3p_2 - 1)^3} - \tilde{p}}} - \frac{i\sqrt{3} + 1}{6} \cdot \sqrt[3]{\sqrt{\tilde{p}^2 - (3p_3p_2 - 1)^3} - \tilde{p}}. \tag{27}$$

Summing up, we deduce the following.

Proposition 1. *Any small zero of the zeta function $Z_{\mathbb{T}(a)}$ is close to a solution of one of the twelve equations*

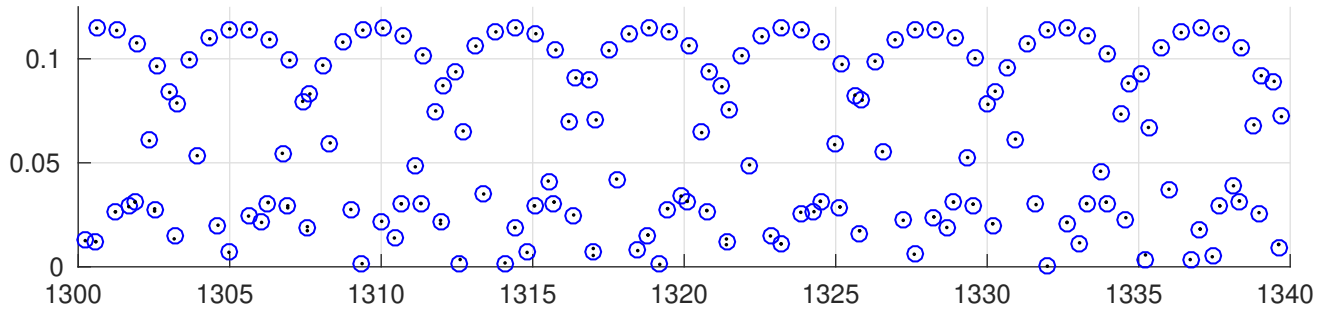
$$\exp(2as) = \lambda_j(p_1(s), p_2(s), p_3(s)), \quad j = 1, \dots, 12, \tag{28}$$

where λ_k , $k = 1, \dots, 12$ are given by (22)–(27).

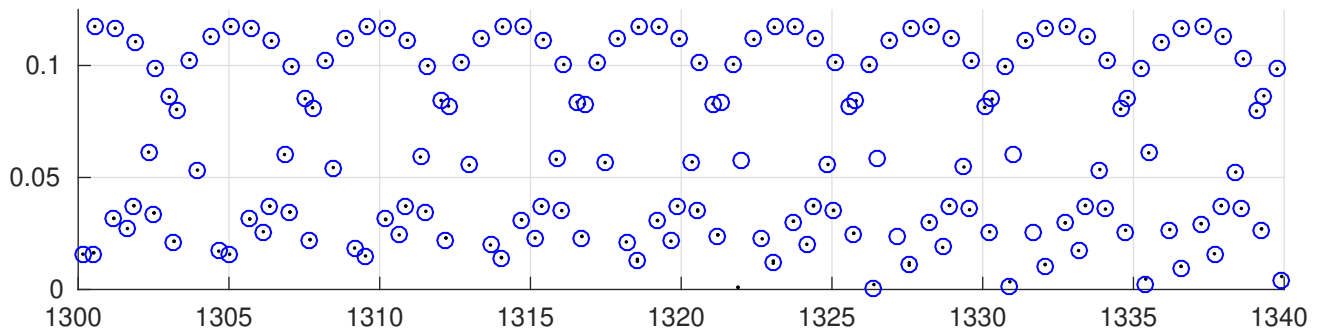
We omit the proof here. Figure 19 shows the small zeros of the zeta function along with the zeros of the determinant.

In the next section we discuss properties of solutions of equations (28), or in other words, zeros of the determinant $\det(I - \exp(-2as)P(s))$.

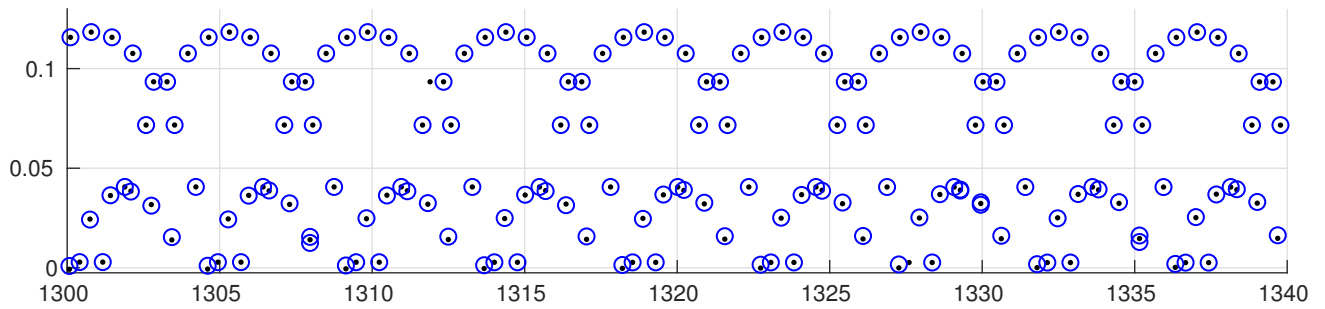
Figure 19: Zeros of the determinant $I - \exp(-2as)P(s)$ (circles) and zeros of the zeta function (dots) in a small part of the critical strip $1300 < \Re z < 1340$. In the cases we consider $\exp(\frac{3a}{2}) \approx 1400$.



(a) The case of $\mathring{\mathbb{T}}(10)$.



(b) The case of $\mathring{\mathbb{T}}(14 \log 2 + 0.05)$.



(c) The case of $\mathring{\mathbb{T}}(14 \log 2)$.

8.2.4 Zeros of the determinant

Solving $\lambda_{1,2}(s) = \exp 2as$. The first two eigenvalues have a simple form as functions of s and equation (28) gives us two equations:

$$\exp(2as) = \pm 2^{s+1} \sinh(2se^{-2a}). \quad (29)$$

We may write $s = \sigma + it$ and use the equality between squares of the absolute values

$$|\exp((2a - \log 2)s)|^2 = |\sinh(2se^{-2a})|^2$$

to obtain

$$\exp((2a - \log 2)2\sigma) = \exp(4\sigma e^{-2a}) + \exp(-4\sigma e^{-2a}) - 2 \cos(4te^{-2a}),$$

which implies

$$t = \frac{e^{2a}}{4} \left(\pm \arccos \left(-\frac{1}{2} \exp((2a - \log 2)2\sigma) + \cosh(4\sigma e^{-2a}) \right) + 2\pi k \right), \quad (30)$$

provided

$$\left| \frac{1}{2} \exp((2a - \log 2)2\sigma) - \cosh(4\sigma e^{-2a}) \right| \leq 1.$$

Since for small σ we have that $\cosh(4\sigma e^{-2a}) = 1 + 4\sigma^2 e^{-4a} + o(e^{-6a})$, the above condition is valid provided $\sigma < \frac{\log 2}{2a - \log 2}$. However, for positive real part $\sigma > 0$ we have that imaginary part $t > \frac{1}{4}e^{2a}$, which is outside of the range of small zeros. Hence we have established the following.

Lemma 24. *The first two eigenvalues (22) don't give any information on location of small zeros in positive half-plane.*

The equality (29) also implies the equality between arguments:

$$\arg(\exp((2a - \log 2)s)) = \arg(\sinh(2se^{-2a})).$$

We see that for $s = \sigma_0 + it$ the function $\arg(\sinh(2se^{-2a}))$ is monotone increasing and small, while $\arg(\exp((2a - \log 2)s))$ is changing rapidly. We therefore expect that solutions of (29) with $|s| < e^{2a}$ belong to the curve given by (30) and the difference between imaginary parts of consecutive zeros is approximately $\frac{2\pi}{2a - \log 2}$.

We now proceed to analyse the equations coming from the next four eigenvalues.

Solving $\lambda_{3,4}(s) = \exp 2as$ and $\lambda_{5,6}(s) = \exp 2as$. The equations (28) read

$$2e^{2as} = 1 - 2^{s+1} \cosh(2se^{-2a}) \pm \sqrt{(2^{s+1} \cosh(2se^{-2a}) + 1)^2 - 2^{s+3}}; \quad (31)$$

$$2e^{2as} = 1 + 2^{s+1} \cosh(2se^{-2a}) \pm \sqrt{(2^{s+1} \cosh(2se^{-2a}) - 1)^2 + 2^{s+3}}; \quad (32)$$

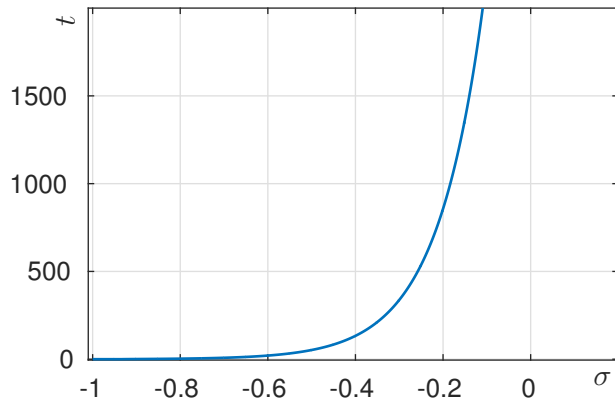


Figure 20: A plot of imaginary part $\Im(s) = t$ as a function of the real part $\Re(s) = \sigma$ as defined by (30). The zeros of the determinant $\det(I - A(s))$ defined by $\lambda_{1,2} = \exp(2as)$ are outside of the domain of approximation.

which is equivalent to

$$\begin{aligned} e^{2as} (e^{2as} \cdot 2^{-s-1} - 2^{-s-1} + \cosh(2se^{-2a})) &= \cosh(2se^{-2a}) - 1, \\ e^{2as} (e^{2as} \cdot 2^{-s-1} - 2^{-s-1} - \cosh(2se^{-2a})) &= 1 - \cosh(2se^{-2a}). \end{aligned}$$

The determinant $\det(I - \exp(-2as)P(s))$ approximates the zeta function on a part of the critical strip $0 < \Re(s) < \delta$, $0 < \Im(s) < e^{\frac{3a}{2}}$. We have the following asymptotic expansion for the right hand side:

$$\begin{aligned} |\cosh(2se^{-2a}) - 1| &\leq \sum_{j=1}^{\infty} |4^j e^{-4aj} s^{2j}| = \sum_{j=1}^{\infty} 4^j e^{-4aj} (\sigma^2 + t^2)^j \\ &\leq 4e^{-4a}(\sigma^2 + t^2) + \frac{16e^{-8a}(\sigma^2 + t^2)^2}{1 - 4(\sigma^2 + t^2)e^{-4a}}. \end{aligned} \quad (33)$$

This allows us to deduce that zeros of the zeta function with imaginary part $\Im(s) = |t| \leq e^{\frac{3a}{2}} \approx 1800$ are close to solutions of the approximate equations

$$e^{2as} \cdot 2^{-s-1} - 2^{-s-1} + 1 = 0, \quad (34)$$

$$e^{2as} \cdot 2^{-s-1} - 2^{-s-1} - 1 = 0. \quad (35)$$

Evidently solutions of (34) and (35) should satisfy

$$|e^{2as}|^2 = |2^{s+1} - 1|^2 \text{ and } |2^{s+1}|^2 = |e^{2as} - 1|^2; \text{ or} \quad (36)$$

$$|e^{2as}|^2 = |2^{s+1} + 1|^2 \text{ and } |2^{s+1}|^2 = |e^{2as} - 1|^2. \quad (37)$$

and therefore belong to the intersections $\mathcal{T}_1 \cap \mathcal{T}_2$ of the of curves given by

$$\mathcal{T}_1 \stackrel{\text{def}}{=} \left\{ \sigma + it \mid \cos(2at) = \pm \frac{1 + e^{2a\sigma} - 4^{1+2\sigma}}{2e^{2a\sigma}} \right\} \quad (38)$$

$$\mathcal{T}_2 \stackrel{\text{def}}{=} \left\{ \sigma + it \mid \cos(t \log 2) = \pm \frac{4^{1+2\sigma} + 1 - e^{4a\sigma}}{4^{1+\sigma}} \right\}. \quad (39)$$

We summarize our findings in the following

Lemma 25. *There exist a zero of the zeta function $\zeta_{\mathbb{T}(a)}$ in e^{-a} -neighbourhood of every **odd** element of the following subsequences of the points of intersection with $\Im z_n < e^{\frac{3a}{2}}$ (see plots in Figure 21)*

$$z_n = \sigma_n + it_n \text{ where } \cos(2at_n) = \frac{1 + e^{2a\sigma_n} - 4^{1+2\sigma_n}}{2e^{2a\sigma_n}}, \cos(t_n \log 2) = \frac{e^{4a\sigma_n} - 4^{1+2\sigma_n} - 1}{2^{2+\sigma_n}} \text{ and } t_n < t_{n+1};$$

$$z_n = \sigma_n + it_n \text{ where } \cos(2at_n) = \frac{4^{1+2\sigma_n} - 1 - e^{2a\sigma_n}}{2e^{2a\sigma_n}}, \cos(t_n \log 2) = \frac{e^{4a\sigma_n} - 4^{1+2\sigma_n} - 1}{2^{2+\sigma_n}} \text{ and } t_n < t_{n+1}.$$

Corollary 3. *In the case $a \in \mathbb{N} \log 2$ solutions to this system belong to the straight lines $\Im z = \sigma = \text{const}$; moreover, the intersection of the zero set with any of this lines is a periodic set of period $\frac{2\pi}{\log 2}$. These lines correspond to seemingly straight lines we see in Figure 14(c). In the case $a \notin \mathbb{N} \log 2$ this no longer holds and we see a random structure as shown in Figure 14(a).*

Analysing $\lambda_{7,8}(s) = \exp(2as)$ Let us now consider the remaining eigenvalues $|\exp(2as)| = |\lambda_k(s)|$, $7 \leq k \leq 12$. The explicit expressions (25), (26) and (27) can be used to compute the curves where the zeros are located numerically. It turns out that equation (28) have solutions in the domain of approximation only for $k = 7, 8$. In Figure 22(a) we see a part of the curve defined by

$$\mathcal{T}_3 = \{s = \sigma + it \mid |\exp(2as)| = |\lambda_k(s)|\} \quad (40)$$

for $k = 7, 8$; Figures 22(b) and 22(c) show two pieces of the curve corresponding to $0 < \Im s < 20$ and $310 < \Im s < 340$ with zeros of the zeta function located there.

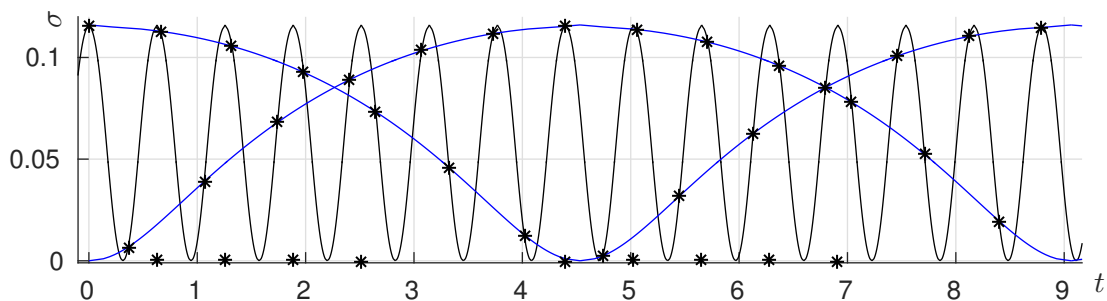
In an attempt to find a transversal family of curves that would help to describe the location of the zeros more precisely, we would like to study the polynomial

$$\prod_{j=7}^{12} (x - \lambda_j(s)) = \det(P(s) - xI) \cdot \prod_{j=1}^6 (x - \lambda_j(s))^{-1}.$$

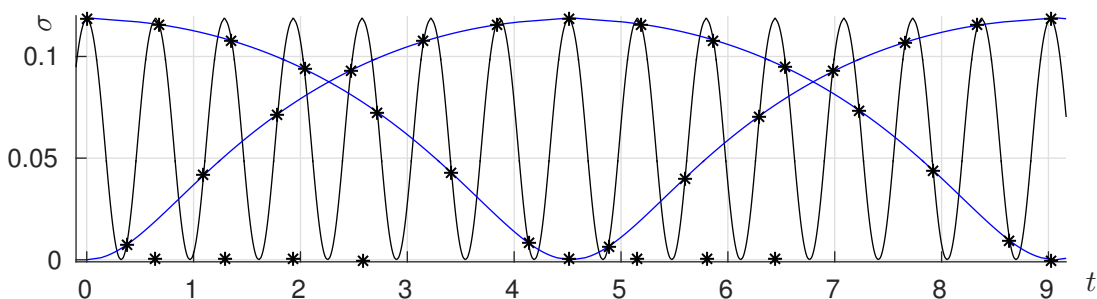
By a straightforward calculation we obtain

$$\prod_{j=7}^{12} (x - \lambda_j(s)) = (x^3 - x^2 + p_2 p_3 x + (2p_1^2 - p_2) p_3)^2. \quad (41)$$

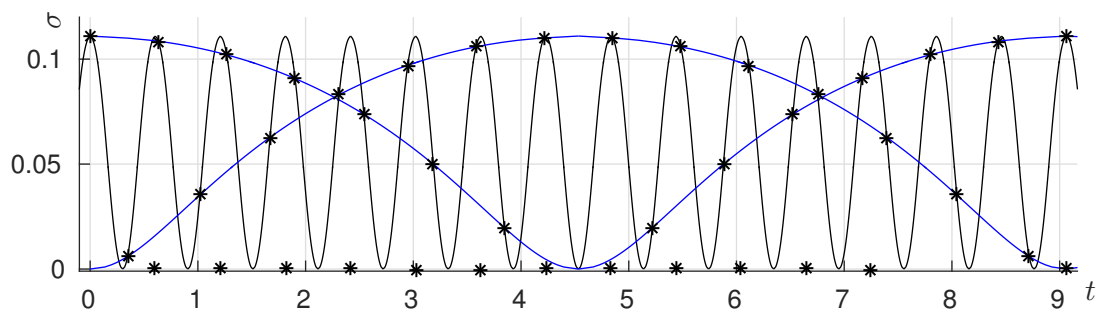
Figure 21: Families of curves \mathcal{T}_1 quickly oscillating with period $\frac{\pi}{a}$ and \mathcal{T}_2 slowly oscillating with period $\frac{2\pi}{\log 2}$ as defined by (38) and (39) and described in Lemma 25 and zeros of the 12th Taylor polynomial approximating the zeta function (stars). We see that the actual zeros occur very close to odd elements of the sequences of points of intersections. Zeros on the imaginary axis correspond to solutions of $e^{2as} = \lambda_{7,8}(s)$.



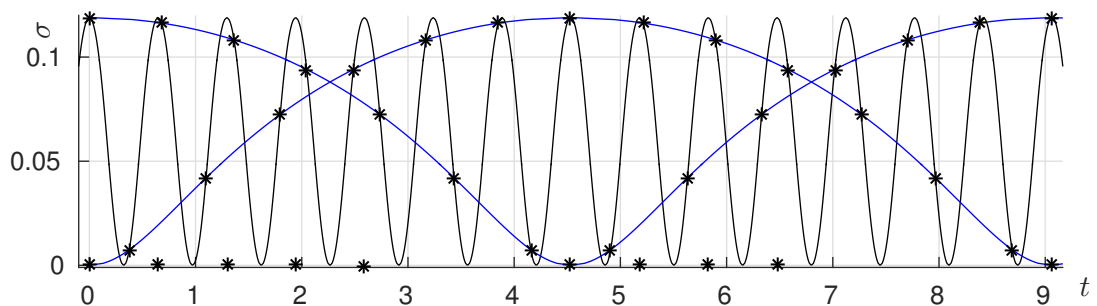
(a) Case $a = 10$. A part of the zero set from Figure 14(a).



(b) Case $a = 14 \log 2 + 0.05$. A part of the zero set from Figure 14(b).



(c) Case $a = 14 \log 2$. A part of the zero set from Figure 14(c). The real and the imaginary axis are swapped. The nearly straight lines would correspond to $\sigma = \text{const}$.



(d) Case $a = 15 \log 2$. Together with the plot above they illustrate Corollary 3.

We would like to return to the original variable s , i.e. to reverse (19)–(21), taking into account that for $\Re(s) \ll 1$ we have that $\sinh(s) \approx i \sin(t)$ and $\cosh(s) \approx \cos(t)$:

$$p_1(s) \approx 2^{\frac{s}{2}}; \quad (42)$$

$$p_2(s) \approx 2^{s+1} \cos(2te^{-2a}); \quad (43)$$

$$p_3(s) \approx 2^{s+1} \sin(2te^{-2a})i. \quad (44)$$

We obtain an approximation

$$\prod_{j=7}^{12} (x - \lambda_j(s)) \approx (x^3 - x^2 + i2^{2s+1} (\sin(4e^{-2a}t)(x-1) + 2 \sin(2e^{-2a}t)))^2.$$

The latter implies

$$2^{4\sigma+2} = |2^{2s+1}|^2 = \left| \frac{(x^3 - x^2)}{(\sin(4e^{-2a}t)(x-1) + 2 \sin(2e^{-2a}t))} \right|^2. \quad (45)$$

Substituting $x = \exp(2as)$ we solve the equation for $\cos(2at)$ and obtain the equality

$$\cos(2at) = \frac{e^{8a\sigma}(e^{4a\sigma} + 1) - 2^{4\sigma+2} (\sin^2(4e^{-2a}t)(e^{4a\sigma} + 1) - 2 \sin(4e^{-2a}t) + 4 \sin^2(2e^{-2a}t))}{2e^{2a\sigma} (2^{4\sigma+2}(\sin(4e^{-2a}t) - \sin^2(4e^{-2a}t)) + e^{8a\sigma})}. \quad (46)$$

We see that although the right hand side depends on t , and as t varies in any small interval of length $c \ll \exp(a)$, say $(nc, (n+1)c)$ the dependence on t is negligible, so we may consider a partition into intervals of length c and the curves defined by

$$\mathcal{J}_4 = \left\{ \sigma + it \mid \cos(2at) = \frac{e^{8a\sigma}(e^{4a\sigma+1}) - 2^{4\sigma+2} (\sin^2(4e^{-2a}nc)(e^{4a\sigma} + 1) - 2 \sin(4e^{-2a}nc) + 4 \sin^2(2e^{-2a}nc))}{2e^{2a\sigma} (2^{4\sigma+2}(\sin(4e^{-2a}nc) - \sin^2(4e^{-2a}nc)) + e^{8a\sigma})} \right\} \quad (47)$$

on the intervals $nc < t < (n+1)c$, $n \in \mathbb{Z}$.

Remark 6. The dependence of the right hand side on t is reflected in increasing amplitude of oscillations of the curve in Figure 22(a). It is possible to make further simplification of the right hand side of (47), using first order approximations $\sin(x) \approx x$ and $\cos(x) \approx 1$ for small x . This would lead to

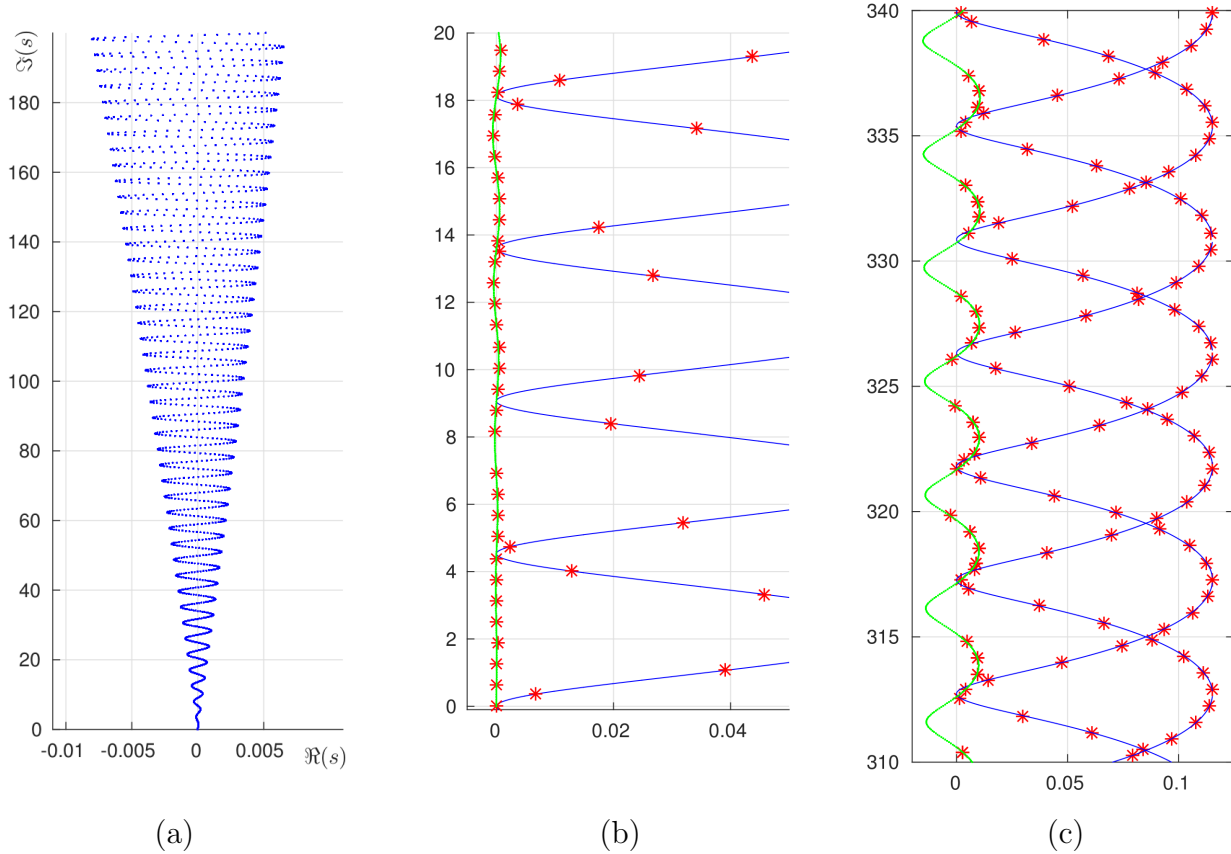
$$\mathcal{J}'_4 = \left\{ \sigma + it \mid \cos(2at) = \frac{e^{8a\sigma}(e^{4a\sigma} + 1) - 2^{4\sigma+5}e^{-2a}t(2e^{-2a}t(e^{4a\sigma} + 2) - 1)}{2e^{2a\sigma}(2^{4\sigma+4}e^{-2a}t(1 - 4e^{-2a}t) + e^{8a\sigma})} \right\}. \quad (48)$$

It is evident that the plot will be a quickly oscillating curve with period $\frac{\pi}{a}$ and increasing amplitude of oscillations.

We summarize our discussion in this section as follows.

Proposition 2. *Zeros of the zeta function in the critical strip with imaginary part $\Im s < e^a$ are e^{-a} -close either to the intersections $\mathcal{J}_1 \cap \mathcal{J}_2$, as described in Lemma 25 or to the intersections $\mathcal{J}_3 \cap \mathcal{J}_4$.*

Figure 22: Several plots showing the curve $|\exp(2as)| = |\lambda_{7,8}(s)|$. (a) General plot of the curve within the rectangle $-0.01 < \Re s < 0.01$, $0 < \Im s < 200$; (b) A part of the curve near the real axis $-0.005 < \Re s < 0.05$, $0 < \Im s < 20$, stars mark zeros of the zeta function, the oscillating curve in horizontal direction is \mathcal{T}_2 ; (c) The curve in the part of the critical strip $0 < \Re s < \delta$, $310 < \Im s < 340$, oscillating around imaginary axis. Stars mark zeros of the zeta function. The second oscillating curve is \mathcal{T}_2 .



References

- [1] Adler, R. Afterword to “Invariant measures for Markov maps of the interval” by R. Bowen, *Comm. Math. Phys.* 69 (1979), no. 1, 1–17.
- [2] Adler, R. and Flatto, L. Geodesic flows, interval maps, and symbolic dynamics *Bull. Amer. Math. Soc. (N.S.)* Volume 25, Number 2 (1991), 229–334.
- [3] Beardon, A. F. *The geometry of discrete groups*. Graduate Texts in Mathematics, 91. Springer-Verlag, New York, 1995. xii+337 pp.
- [4] Bedford, T., Keane, M. and Series, C., *Ergodic theory, Symbolic Dynamics and Hyperbolic Spaces*, C.U.P., Oxford, 1989, 384pp.
- [5] Borthwick, D. Distribution of resonances for hyperbolic surfaces. *Exp. Math.* 23 (2014), no. 1, 25–45.
- [6] Borthwick, D. *Spectral Theory of Infinite-Area Hyperbolic Surfaces*, second ed., *Progr. Math.* 318, Birkhäuser/Springer, [Cham], 2016
- [7] Bowen, R, and Series, C. Markov maps associated with fuchsian groups *Publications mathématiques de l’I.H.É.S.*, tome 50 (1979), p. 153–170
- [8] Borthwick, D. and Weich, T. Symmetry reduction of holomorphic iterated function schemes and factorization of Selberg zeta functions, *J. Spectral Theory*, 6 (2016) 267–329.
- [9] Buser, P. *Geometry and spectra of compact Riemann surfaces*, Birkhäuser, Boston, 1992.
- [10] Buser, P. and Semmler, K.-D. The geometry and spectrum of the one holed torus. *Commentarii mathematici Helvetici* 63.2 (1988): 259–274
- [11] Cheeger, J. A lower bound for the smallest eigenvalue of the Laplacian. *Problems in analysis (Papers dedicated to Salomon Bochner, 1969)*, 195–199. Princeton Univ. Press, Princeton, N. J., 1970.
- [12] Dolgopyat, D. On decay of correlations in Anosov flows. *Ann. of Math. (2)* 147 (1998), no. 2, 357–390.
- [13] Dyatlov, S. Improved fractal Weyl bounds for hyperbolic manifolds. with an appendix by David Borthwick, Semyon Dyatlov and Tobias Weich. *Journal of the European Mathematical Society*, 21(6):1595–1639, Feb 2019.
- [14] Dyatlov, S. and Zworski, M. *Mathematical Theory of Scattering Resonances*, in *Graduate Studies in Mathematics* (American Mathematical Society, Providence, 2019).

- [15] Falconer, K. *Fractal geometry. Mathematical foundations and applications*. John Wiley & Sons, Ltd., Chichester, 1990, xxii+288pp.
- [16] Ford, L. R. *Automorphic Functions*. New York, McGraw-Hill, 1929. vii+333pp.
- [17] Grothendieck, A. Produits tensoriels topologiques et espaces nucléaires. (French) Mem. Amer. Math. Soc. No. 16 (1955), 140pp.
- [18] Grothendieck, A. La théorie de Fredholm. Bull. Soc. Math. France 84 (1956), 319–384.
- [19] Hejhal, D. *The Selberg Trace Formula for $PSL(2, \mathbb{R})$* , Lecture Notes in Mathematics 548, Springer, Berlin, 1976.
- [20] Huber, H. Zur analytischen Theorie hyperbolischen Raumformen und Bewegungsgruppen (I), Math. Ann. 138 (1959), 1–26.
- [21] Huber, H. Zur analytischen Theorie hyperbolischen Raumformen und Bewegungsgruppen (II), Math. Ann. 142 (1961), 385–398.
- [22] Margulis, G. A. On some aspects of the theory of Anosov systems, in Springer Monographs in Mathematics (Springer-Verlag, Berlin, 2004). With a survey by Richard Sharp: Periodic orbits of hyperbolic flows, Translated from the Russian by Valentina Vladimirovna Szulikowska.
- [23] Mayer, D. H. Continued fractions and related transformations. Ergodic theory, symbolic dynamics, and hyperbolic spaces (Trieste, 1989), 175–222, Oxford Sci. Publ., Oxford Univ. Press, New York, 1991.
- [24] McKean, H. Selberg’s trace formula as applied to a compact Riemann surface. Comm. Pure Appl. Math. 25 (1972), 225–246
- [25] McMullen, C. T. Hausdorff dimension and conformal dynamics. III. Computation of dimension. Amer. J. Math. 120 (1998), no. 4, 691–721.
- [26] Moore, C. C. Exponential decay of correlation coefficients for geodesic flows. Group representations, ergodic theory, operator algebras, and mathematical physics (Berkeley, Calif., 1984), 163–181, Math. Sci. Res. Inst. Publ., 6, Springer, New York, 1987.
- [27] Naud, F. Expanding maps on Cantor sets and analytic continuation of zeta functions, Ann. Sci. Ecole Norm. Sup. 38 (2005), 116–153.
- [28] Naud, F. Density and location of resonances for convex co-compact hyperbolic surfaces. Invent. Math. 195 (2014), no. 3, 723–750.
- [29] Nicholls, P. J. *The ergodic theory of discrete groups*, LMS–LNS 143, C.U.P., Cambridge 1990;

-
- [30] Parry, W. and Pollicott, M. Zeta functions and the periodic orbit structure of hyperbolic dynamics. *Astérisque* No. 187–188 (1990), 268pp.
- [31] Pollicott, M. Some applications of thermodynamic formalism to manifolds with constant negative curvature. *Adv. Math.* 85 (1991), no. 2, 161–192.
- [32] Pollicott, M. Meromorphic extensions of generalised zeta functions. *Invent. Math.* 85 (1986), no. 1, 147–164.
- [33] Pollicott, M. On the rate of mixing of Axiom A flows. *Invent. Math.* 81 (1985), no. 3, 413–426.
- [34] Pollicott, M. and Vytnova, P., Zeros of the Selberg zeta function for symmetric infinite area hyperbolic surfaces, *Geom. Dedicata* 201 (2019) 155–186.
- [35] Ruelle, D. Zeta-functions for expanding maps and Anosov flows. *Invent. Math.* 34 (1976), no. 3, 231–242.
- [36] Schoen, R.; Wolpert, S.; Yau, S. T. Geometric bounds on the low eigenvalues of a compact surface. *Geometry of the Laplace operator (Proc. Sympos. Pure Math., Univ. Hawaii, Honolulu, Hawaii, 1979)*, pp. 279–285, *Proc. Sympos. Pure Math.*, XXXVI, Amer. Math. Soc., Providence, R.I., 1980.
- [37] Selberg, A. Harmonic analysis and discontinuous groups in weakly symmetric Riemannian spaces with applications to Dirichlet series. *J. Indian Math. Soc. (N.S.)* 20 (1956), 47–87.
- [38] Series, C. Geometrical Markov coding of geodesics on surfaces of constant negative curvature, *Ergod. Th. and Dynam. Sys.*, 6 (1986) 601–625
- [39] Series, C. The geometry of Markoff numbers. *Math. Intelligencer* 7 (1985), 20–29.
- [40] Weich, T. Resonance chains and geometric limits on Schottky surfaces. *Comm. Math. Phys.* 337 (2015), no. 2, 727–765.